

## ABSTRACT

### Adaptive Radar Waveform Synthesis via Alternating Projections

Dylan Eustice, M.S.E.C.E.

Mentor: Charles P. Baylis II, Ph.D.

As the number of wireless broadband devices occupying our airwaves grows at a rapid rate, the resultant decrease in available spectrum for current technologies and increasingly stringent regulations on band compliance has necessitated adaptive radio frequency (RF) technologies which can respond to the spectrum crisis. The task of maintaining the effectiveness of our RF technology with a shrinking spectrum has generated work in a number of fields, notably cognitive radar. This work focuses on developing an algorithm which can adaptively produce waveforms with desired accuracy in the range-Doppler domain, measured by the ambiguity function, for radar detection while also having characteristics which allow for efficient amplifier operation and spectral compliance.

Adaptive Radar Waveform Synthesis via Alternating Projections

by

Dylan Eustice, B.S.E.C.E.

A Thesis

Department of Electrical and Computer Engineering

---

William Jordan, Ph.D., Chairperson

Submitted to the Graduate Faculty of  
Baylor University in Partial Fulfillment of the  
Requirements for the Degree  
of

Master of Science in Electrical and Computer Engineering

Approved by the Thesis Committee

---

Charles P. Baylis II, Ph.D.

---

Robert J. Marks II, Ph.D.

---

Brian A. Garner, Ph.D.

Accepted by the Graduate School

December 2015

---

J. Larry Lyon, Ph.D., Dean

Copyright © 2015 by Dylan Eustice

All rights reserved

## TABLE OF CONTENTS

LIST OF FIGURES	v
LIST OF TABLES	vii
ACKNOWLEDGMENTS	viii
CHAPTER ONE: INTRODUCTION	1
CHAPTER TWO: BACKGROUND	3
2.1    Background of the Ambiguity Function	3
2.1.1    Mathematical Interpretation	3
2.1.2    Notable Properties of the Ambiguity Function	5
2.2    Background of Projection onto Convex Sets	7
2.3    Prior Art	11
CHAPTER THREE: FUNDAMENTAL PROJECTIONS FOR WAVEFORM DESIGN	14
3.1    Overview of Projections	14
3.1.1    The Minimization Function	14
3.1.2    Projections to the Time Domain	18
3.2    Distance Functions	23
3.3    Results and Conclusions	24
3.3.1    Results	24
3.3.2    Conclusions	36
CHAPTER FOUR: DESIGNING FOR ADDITIONAL WAVEFORM CONSIDERATIONS	37
4.1    Considering PAPR and Spectrum	38
4.1.1    Importance in Waveform Design	38
4.2    Projections for PAPR and Spectrum	39
4.2.1    Projections to Ensure Desired PAPR	40
4.2.2    Projections to Ensure Desired Spectrum	41
4.2.2    Ensuring Both Desired Spectrum and Desired PAPR	43
4.3    Results and Conclusions	44
4.3.1    Results	44
4.3.2    Conclusions	54
CHAPTER FIVE: CONCLUSIONS	56
BIBLIOGRAPHY	59

## LIST OF FIGURES

Figure 1: An example of POCS convergence.	8
Figure 2: Disagreement between waveform calculations.	161
Figure 3: Examples of possible minimization functions.	16
Figure 4: An example of the projection to minimized function.	18
Figure 5: Simulated mean-squares optimization result for trial I.	277
Figure 6: Simulated mean-squares optimization result for trial II.	288
Figure 7: Simulated mean-squares optimization result for trial III.	29
Figure 8: Simulated mean-squares optimization result for trial IV.	30
Figure 9: Measured mean-squares optimization result for trial I.	31
Figure 10: Measured mean-squares optimization result for trial II.	32
Figure 11: Measured mean-squares optimization result for trial III.	33
Figure 12: Measured mean-squares optimization result for trial IV.	34
Figure 13: Convergence in Trials II and III for both mean-square and minimax.	35
Figure 14: An example of compliant and noncompliant spectra.	42
Figure 15: Spectrum of a notched waveform.	43
Figure 16: Simulated mean-squares optimization result for trial I.	46
Figure 17: Simulated mean-squares optimization result for trial II.	47
Figure 18: Simulated mean-squares optimization result for trial III.	48
Figure 19: Simulated mean-squares optimization result for trial IV.	49
Figure 20: Measured mean-squares optimization result for trial I.	50
Figure 21: Measured mean-squares optimization result for trial II.	51

Figure 22: Measured mean-squares optimization result for trial III. 52

Figure 23: Measured mean-squares optimization result for trial IV. 53

## LIST OF TABLES

Table 1: Summary of Chapter Three results.	26
Table 2: Summary of Chapter Four results.	45

## ACKNOWLEDGMENTS

This work would not have been possible without a fantastic support system from my colleagues in the WMCS lab. I want to thank my advisor, Dr. Charles Baylis, for providing the opportunity to pursue my graduate studies, for always pushing me to my fullest potential, and for constantly being an enthusiastic resource, Dr. Robert Marks for his unending intellectual stimulation, support, and bottomless supply of personal anecdotes, and Larry Cohen from the Naval Research Labs for his continued insight and contributions to our work. Thanks also to Matthew Fellows for his previous work on the project which paved the way for my research, to Joe Barkate, my fellow Masters student, and to our invaluable undergraduate assistants. Special thanks also to the National Science Foundation for funding this work under grant number ECCS-1343316.

Most of all I would like to thank my parents, Scott and Sally Eustice, for their unwavering support, love, and encouragement, without which I wouldn't be the man I am today and to my brother and sister, Mason and Morgan, for their support. Finally, I want to thank the innumerable people in my life that I've been lucky enough to call friends, and whom I care for deeply.

## CHAPTER ONE

### Introduction

As wireless technology advances, the density of wireless applications in the available spectral range has skyrocketed while the demand for performance has increased significantly as well. In order to accommodate the increase of devices entering the spectrum, new, increasingly stringent, spectral restrictions have been placed on both current technologies and new devices. Additionally, the United States government has instituted provisions which are intended to regulate the spectral sharing needed to allow the spectral cooperation of wireless devices. The largest piece of evidence regarding the new emphasis on spectral sharing has been the National Broadband Plan from 2010, which required 500 MHz of government controlled spectrum to be auctioned to the commercial sector by 2020. A great deal of that spectrum will be taken from military applications, notably radar, which will leave our military to perform the same tasks with less spectrum. The decrease in available spectrum and increasing restrictions on spectral spreading affect radar in two main ways: higher waveform power, which is often associated with increased spectral spreading, is desired to insure targets are sufficiently “illuminated” and to maximize the efficiency of the transmitter and higher bandwidth is often desirable for better radar waveform resolution.

One growing field which has attempted to address this problem is cognitive radar, which attempts to make radar systems adaptable to their environment and constraints. In order to make such a field become practically useful, there need to be algorithms which direct the adaptations of different components of radar systems depending on system

current needs and requirements. This thesis attempts to address and provide a solution for a large problem in radar systems with limited spectrum: how can a radar system provide desirable range-Doppler resolution in a changing environment with limited spectrum? Presented is a projections algorithm which synthesizes waveforms whose range-Doppler resolution properties have been optimized for the current environment. It allows the radar systems operator to select regions in the range-Doppler plane for which to minimize the magnitude of ambiguity function of synthesized waveform, while also ensuring that peak-to-average power ratio and spectrum requirements are met. The inputs to the finalized algorithm are: a two-dimensional function specifying where to minimize the ambiguity function, the energy of the desired waveform, the desired peak-to-average power ratio of the waveform, and a spectral mask which the waveform's frequency spectrum must comply.

Chapter Two provides background on the mathematical theory upon which the projections algorithm is based, as well as state of the art in related literature. Chapter Three formulates the projections used to optimize a waveform based on desired ambiguity function characteristics. Finally, Chapter Four shows how peak-to-average power ratio and spectrum requirements are enforced, while still optimizing the waveform's ambiguity function. Chapter Five presents conclusions and discusses possible future directions for this work.

## CHAPTER TWO

### Background

In order to more properly convey both the technical aspects in the chapters which follow and the overall significance of the work, a background of the related fields will first be provided. Section 2.1 will give an overview of the ambiguity function, with Section 2.1.1 discussing its mathematical interpretation and Section 2.1.2 covering some of its more important properties. Section 2.2 gives a mathematical overview of the projections theory on which the work is based, and Section 2.3 covers prior work done in related fields.

#### *2.1 Background of the Ambiguity Function*

##### *2.1.1 Mathematical Interpretation*

First derived by Woodward [1], the ambiguity function (AF) is a two-dimensional function describing the detection capabilities of a temporal waveform. There is a great amount of literature describing the AF in its many forms, which include the monostatic case [1], the bistatic case [2], narrowband AF [1], wideband AF [3] [4], and ultra-wideband AF [5]. For the purposes of this work, we will consider a narrowband, monostatic radar system and the subsequent AF definition used in this application.

The AF is mathematically defined as

$$\chi(\tau, u) = \int_{-\infty}^{\infty} x(t)x^*(t - \tau)e^{-j2\pi ut} dt \quad (1)$$

where  $\tau$  and  $u$  are the range and Doppler errors relative to the range and Doppler of the detected target, which is centered at the origin in the AF's range-Doppler plane. An

equivalent definition of the AF in the frequency domain can be written by using the Fourier Transform of  $x(t)$ , whose derivation follows. Start by rewriting (1) as

$$\chi(\tau, u) = \int_{-\infty}^{\infty} (x(t)e^{-j2\pi ut}) \cdot (x^*(t - \tau))dt$$

and note the Fourier relationships

$$x(t)e^{-j2\pi ut} \leftrightarrow X(f + u)$$

$$x(t - \tau) \leftrightarrow X(f)e^{-j2\pi f\tau}$$

We then use the power theorem [6], which states that for any signals  $a(t)$  and  $b(t)$  and their Fourier pairs  $A(f)$  and  $B(f)$ ,

$$\int_{-\infty}^{\infty} a(t)b^*(t)dt = \int_{-\infty}^{\infty} A(f)B^*(f)df \quad (2)$$

By setting the above  $a(t) = x(t)e^{-j2\pi ut}$  and  $b(t) = x^*(t - \tau)$  we take advantage of the power theorem,

$$\int_{-\infty}^{\infty} (x(t)e^{-j2\pi ut}) \cdot (x^*(t - \tau))dt = \int_{-\infty}^{\infty} (X(f + u)) \cdot (X^*(f)e^{j2\pi f\tau})df$$

Trivially rearranging terms leads to the alternate definition of the ambiguity function:

$$\chi(\tau, u) = \int_{-\infty}^{\infty} X(f + u)X^*(f)e^{j2\pi f\tau}df \quad (3)$$

In this work, the AF of a specific signal will be referenced by using a subscript notation.

For instance, the AF of signal  $g(t)$  will be given by

$$g(t) \Rightarrow \chi_g(\tau, u)$$

The AF, often referred to as a matched filter [7] [8] due to its foundational basis as a correlator, is a measure of a waveform's range-Doppler resolution, accuracy, and clutter rejection properties relative to a target located at  $(\Delta\tau, \Delta u)$  in the range-Doppler plane [1] [2]. The AF centered at the detected target is given by  $\chi(\tau + \Delta\tau, u + \Delta u)$ .

However, because of the AF's invariance to shifts in time and frequency [8], the AF for a detection at any  $(\Delta\tau, \Delta u)$  may be equivalently written as  $\chi(\tau, u)$ .

There have been many tutorials written about the AF [9] [10] [11], and a more comprehensive overview which develops the AF from basic principles is available in [8]. It should be noted that many authors opt to define the AF as its magnitude, or  $|\chi(\tau, u)|$ . While the real part of the AF is what we desire to maximize when analyzing the AF as a correlator [8], the magnitude of the AF is often the component that is used to assess the quality of the range-Doppler resolution, accuracy, etc [7].

### 2.1.2 Notable Properties of the Ambiguity Function

We will first discuss the extent of the range and Doppler axes which we will consider for the AF, known as the support of the AF. Let a time domain signal  $x(t)$  be constrained on the interval  $t \leq T$  seconds with bandwidth  $B$  Hz. The zero-range and zero-Doppler cuts (setting  $\tau = 0$  and  $u = 0$ ) of the AF are given by the autocorrelation of the waveform and its Fourier transform

$$\begin{aligned}\chi(0, u) &= \int_{-\infty}^{\infty} X(f + u)X^*(f)df = X(u) \star X(u) \\ \chi(\tau, 0) &= \int_{-\infty}^{\infty} x(t)x^*(t - \tau)dt = x(\tau) \star x(\tau)\end{aligned}\tag{4}$$

The support of the ambiguity function along the range axis is assessed by the support of  $x(\tau) \star x(\tau)$ , or  $|\tau| \leq 2T$ , and the support along the Doppler axis is given by the support of  $X(u) \star X(u)$ , which is  $|u| \leq 2B$ .

Throughout this work, the AF of a baseband waveform will be considered. While designing a waveform at baseband is common practice [12] [13] [14], it is notable because it dictates that the signal processing for detections must also be done at

baseband. The proof for this follows. Let the modulated waveform  $s_W(t)$  be uniquely defined by the baseband waveform  $g(t)$  and be expressed as

$$s_W(t) = \Re g(t)e^{j2\pi Wt} \quad (5)$$

Where  $\Re$  is an operator denoting the real part of its operand.  $\chi_{s_W}(\tau, u)$  may then be expressed in terms of  $\chi_g(\tau, u)$  as

$$\begin{aligned} \chi_{s_W}(\tau, u) = & \frac{1}{4} [e^{j2\pi W\tau} \chi_g(\tau, u) + e^{-j2\pi W\tau} \chi_g^*(\tau, -u)] \\ & + \frac{1}{4} [e^{-j2\pi W\tau} \psi_g(\tau, u + 2W) \\ & + e^{j2\pi W\tau} \psi_g^*(\tau, -(u + 2W))] \end{aligned} \quad (6)$$

where  $W$  is the carrier frequency and

$$\psi_g(\tau, u) = \int_{-\infty}^{\infty} g(t)g(t - \tau)e^{-j2\pi ut} dt \quad (7)$$

The derivation of this property may be found in [8]. The  $\psi_g$  terms, which look similar to that of the baseband AF and are called the ‘‘pseudo ambiguity function’’, exist far enough along the Doppler axis such that they may be safely ignored in many situations to be encountered in practice, because these terms will have Doppler frequencies on the order of the carrier frequency. In practice, most moving targets detectable by radar systems will have frequencies much lower than typical radio-frequency carriers. Removing these terms, we are left with

$$\chi_{s_W}(\tau, u) = \frac{1}{4} [e^{j2\pi W\tau} \chi_g(\tau, u) + e^{-j2\pi W\tau} \chi_g^*(\tau, -u)] \quad (8)$$

which is closely related to  $\chi_g(\tau, u)$ , and is in fact simply the baseband AF modulated by the carrier frequency,  $W$ . Because of sampling limitations at typical RF carrier frequencies, this relationship is very important in the formulation of this work.

Computing the AF of waveforms at RF frequencies is extremely computationally expensive due to the number of samples required to accurately represent the waveform. Because of the relationship in (8), the computational complexity may be vastly reduced by downconverting the waveform and computing its AF at baseband. Additionally, we see that our approach of synthesizing the waveform at baseband rather than RF when designing for AF is acceptable, as the two AFs will be virtually indistinguishable at RF frequencies.

## *2.2 Background of Projection onto Convex Sets*

Many problems in engineering and mathematics can be formulated as trying to find an intersection point or a point which is adequately near two or more convex sets. This type of problem is often referred to as the Convex Feasibility Problem [15], which is solved by finding the intersection between a finite number of  $n$ -dimensional sets existing in the Euclidean space  $\mathbb{R}^n$ . Projection onto convex sets (POCS) is a commonly used, simple, and robust method for solving the Convex Feasibility Problem [16] [17] and has been used in a variety of applications [18] [19] [20] [21] [22]. Following the classic definition of convexity [6], a set of signals  $\mathcal{U}$  is convex if and only if

$$\alpha u_1(t) + (1 - \alpha)u_2(t) \in \mathcal{U} \quad (9)$$

for all

$$u_1(t), u_2(t) \in \mathcal{U}$$

$$0 \leq \alpha \leq 1$$

In other words, given any two signals  $u_1(t)$  and  $u_2(t)$  which are in the set  $\mathcal{U}$ ,  $\mathcal{U}$  is convex if and only if the weighted combination of the two signals is also in  $\mathcal{U}$ . Using

POCS, convergence is guaranteed given that all sets  $(\mathcal{U}_1, \mathcal{U}_2, \dots, \mathcal{U}_n)$  are convex and that their intersection is non-empty

$$\mathcal{C} = \mathcal{U}_1 \cap \mathcal{U}_2 \cap \dots \cap \mathcal{U}_n \neq \emptyset \quad (10)$$

POCS works by alternately projecting from one set onto the near point at another set until an intersection or acceptable solution is found. A simple example is shown in Figure 1, where sets  $\mathcal{A}$  and  $\mathcal{B}$  exist in the two-dimensional Euclidean space  $\mathbb{R}^2$  and have a nonempty intersection  $\mathcal{C} = \mathcal{A} \cap \mathcal{B}$ . The objective is to find a point  $x$  existing in  $\mathbb{R}^2$  for which  $x \in \mathcal{A} \cap \mathcal{B}$ . The arbitrary starting value  $x_0$  is initialized at the lowest red circle and the intersection is found at the purple circle. The projections onto  $\mathcal{A}$  and  $\mathcal{B}$  are given by  $P_{\mathcal{A}}$  and  $P_{\mathcal{B}}$ , respectively. The algorithm can then be defined as:

$$x_{n+1} = P_{\mathcal{B}}(P_{\mathcal{A}}(x_n))$$

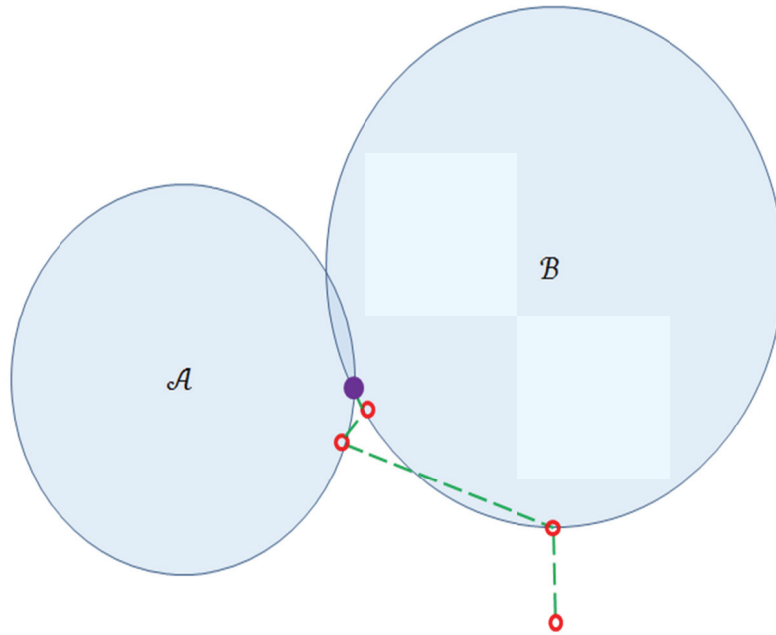


Figure 1: An example of POCS convergence for two sets existing in a two-dimensional Euclidean space. Iterations  $x_0$  through  $x_3$  are shown with red circles, with the intersection point  $x_4$  represented by the purple circle.

Note the projections algorithm to find the intersection for a set of  $n$  sets ( $\mathcal{U}_1, \mathcal{U}_2, \dots, \mathcal{U}_n$ ) will be

$$x_{n+1} = P_{\mathcal{U}_1} \left( P_{\mathcal{U}_2} \left( \dots P_{\mathcal{U}_n} (x_n) \dots \right) \right) \quad (11)$$

It is important to note that the set of functions satisfying all the properties of AF, which will be referred to as  $\mathcal{X}$ , is not a convex set according to the definition in (9). To prove this, insert two ambiguity functions for  $u_1(t)$  and  $u_2(t)$ , where

$$\chi_{u_1}(\tau, u) = \int_t u_1(t) u_1^*(t - \tau) e^{-j2\pi u t} dt$$

$$\chi_{u_2}(\tau, u) = \int_t u_2(t) u_2^*(t - \tau) e^{-j2\pi u t} dt$$

Then, applying the above functions to (9)

$$\begin{aligned} & \alpha \int_t u_1(t) u_1^*(t - \tau) e^{-j2\pi u t} dt + (1 - \alpha) \int_t u_2(t) u_2^*(t - \tau) e^{-j2\pi u t} dt \\ &= \int_t [\alpha u_1(t) u_1^*(t - \tau) e^{-j2\pi u t} + (1 - \alpha) u_2(t) u_2^*(t - \tau) e^{-j2\pi u t}] dt \\ &= \int_t [\alpha u_1(t) u_1^*(t - \tau) + (1 - \alpha) u_2(t) u_2^*(t - \tau)] e^{-j2\pi u t} dt \end{aligned}$$

Assigning a signal  $y(t)$  such that

$$y(t) y^*(t - \tau) = \alpha u_1(t) u_1^*(t - \tau) + (1 - \alpha) u_2(t) u_2^*(t - \tau) \quad (12)$$

yields

$$\int_t y(t) y^*(t - \tau) e^{-j2\pi u t} dt \quad (13)$$

We see that if a  $y(t)$  is found which satisfies (12) for any two signals  $u_1(t)$  and  $u_2(t)$ , the weighted combination of the two functions can be put into the form of (1) and prove the set of AFs are convex. However, there exists no analytic way to solve for a  $y(t)$  which satisfies (12), thus the set of AFs is not convex. This is a weak mathematical proof

and can be supplanted with a practical example. Take two ambiguity functions produced by waveforms

$$u_1(t) = \sin((6 \cdot 10^6)\pi t)$$

$$u_2(t) = \cos((2 \cdot 10^6)\pi t)$$

Plugging their associated AFs into (9), where  $\mathcal{X}$  is the set of AFs, we must show an example where

$$\alpha\chi_{u_1}(\tau, u) + (1 - \alpha)\chi_{u_2}(\tau, u) = \chi_z(\tau, u) \in \mathcal{X}$$

is not true to prove  $\mathcal{X}$  is nonconvex. As will be explained in the next chapter, the time domain waveform associated with a particular AF can be calculated within a scaling constant from the AF. There are two different formulas by which this calculation is done,

$$x(t) = \left[ \frac{1}{x(0)} \int_{-\infty}^{\infty} \chi(-\tau, u) du \right]^*$$

$$x(t) = \mathcal{F}^{-1} \left\{ \frac{1}{X^*(0)} \int_{-\infty}^{\infty} \chi(\tau, u) d\tau \right\}$$

which produce matching signals only if the two dimensional function being operated on is an AF. If these calculations do not agree, the function is not in the set of AFs  $\mathcal{X}$ . We see the disagreement in their respective spectral magnitudes in Figure 2, thus showing an example for which (9) does not hold and proving the set of AFs is nonconvex. For this reason, convergence is not guaranteed when applying the classic POCS methodology to our problem and we apply a generalized variant of POCS, which will be referred to as generalized alternating projections.

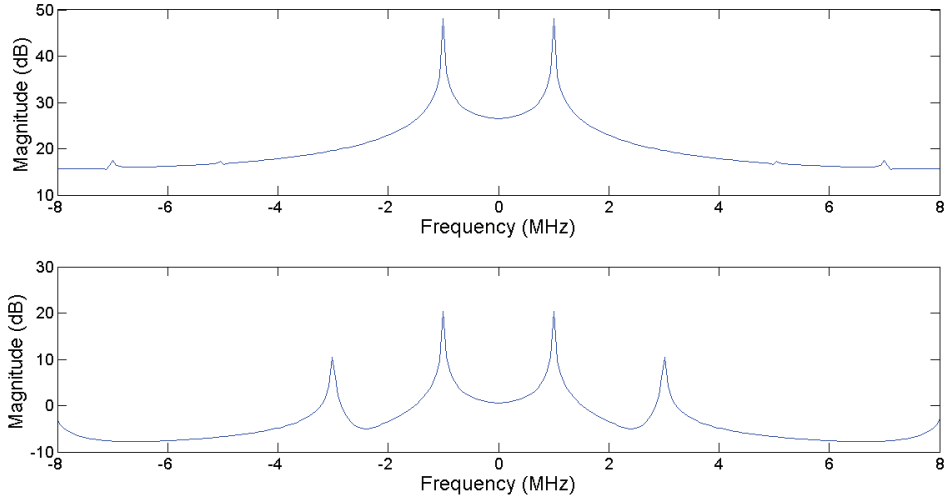


Figure 2: Disagreement in the spectral magnitude between waveform calculations from  $\chi_z(\tau, u)$ , showing the set of AFs is nonconvex.

### 2.3 Prior Art

The topic of synthesizing a waveform optimized for its AF characteristics is an area which has been studied since the early 1960s. It is very important to note that most of the following work is tailored towards developed synthesis for the cross ambiguity function (CAF). The CAF is used in bistatic radar systems as opposed to the AF used in monostatic systems and is defined as

$$\chi_1(\tau, u) = \int_{-\infty}^{\infty} x(t)y^*(t - \tau)e^{-j2\pi ut} dt \quad (14)$$

Notable early work includes that done by Wilcox [23], who devises a least-squares based approach of using a set of basis waveforms to synthesize a waveform whose CAF approximates that of a goal CAF. Sussman [24] and Wolf [25] also provide their own approach to synthesizing a waveform which approximates a desired CAF by utilizing an orthonormal set of basis functions. Gladkova and Chebanov [26] [27] extend Wilcox's method by improving the practicality of creating a goal AF for the algorithm to

approximate. Rather than needing to provide a two dimensional function with all the analytic properties of an AF, their work made it possible to provide a more general two dimensional function to approximate. However, their solution involved using Hermite waveforms, whose generation in practice is not very straightforward [28] [29]. Sebt *et al.* [28] propose a technique to extend Sussman's method using orthogonal frequency division multiplexed (OFDM) waveforms with a lowered peak-to-average power ratio, making their use in radar applications much more practical. Wang *et al.* [30] also derived methods which are used to lower the PAPR in OFDM signals. Additionally, Rowe *et al.* [31] give a fantastic overview of some of the state of the art work being done in waveform design with spectral compliance as a main objective.

Using projections to synthesize waveforms is another technique which has been used previously in literature. Blunt *et al.* use projections to synthesize waveforms in radar embedded communications [32] [33] in work that is tailored towards enabling devices to spectrally coexist. Blunt *et al.* [34] has also recently used projections for spectral and pulse shaping in nonlinear FM chirps. Selesnick and Pillai [35] [36] utilize alternating projections as well, in work in which they demonstrate a method for synthesizing notched chirps. Kassab *et al.* [37] use alternating projections in a fashion similar to our algorithm, however, they focus on optimizing the autocorrelation function of the waveform rather than the AF.

Our work is unique in that it allows a synthesis of a waveform which is not reliant on any set of basis functions and has no prior domain knowledge for waveforms or their associated ambiguity functions, it focuses on the entire supported range-Doppler region

rather than a single correlation, and it provides new metrics on which to judge the quality of an AF against a desired function.

## CHAPTER THREE

### Fundamental Projections for Waveform Design

As previously noted, the waveform synthesis algorithm uses an alternating projections method. This method is based on the theory in the extensive literature pertaining to set and projection theory [38] [39] and the invaluable techniques which have arisen based on their mathematics. This chapter will provide an overview for the foundation of the waveform synthesis algorithm and provide results from the basic algorithm. Section 3.1.1 will introduce the minimization function and demonstrate how to project onto it, Section 3.1.2 demonstrates how to project from the range-Doppler plane to the time domain, Section 3.2 introduces and details the distance functions used, Section 3.3.1 provides a brief recap of the algorithm through this chapter, and Section 3.3.2 provides simulation and measurement results using this method.

#### *3.1 Overview of Projections*

##### *3.1.1 The Minimization Function*

As seen in previous AF synthesis literature [25] [23] [24] [40] [26] [27] [41], it is commonplace to generate an AF which is used as the goal AF for waveform optimization. Most AF synthesis techniques presented in the literature attempt to minimize the mean-square error (MSE) between the AF synthesized and the desired AF. In several works [25] [23] [24], the goal AF must adhere to the analytic properties of AF. Some of these properties [8], notably the energy and area properties shown in (15) and (16), greatly constrain the number of two-dimensional functions which can be used as AF.

$$\int_{\tau} \int_u |\chi_x(\tau, u)|^2 d\tau du = |\chi_x(0,0)|^2 \quad (15)$$

$$\int_{\tau} \int_u \chi_x(\tau, u) d\tau du = x(0)X^*(0) \quad (16)$$

By the energy property (15) we see that the squared magnitude of the origin of the AF is equal to the energy of the AF as a whole. The area property (16) states that the area under the AF is equal to the value of the time domain waveform at  $t = 0$ , multiplied by the value of the conjugate of its Fourier pair at  $f = 0$ .

Because of the specific nature of all the different properties of the AF, in practical applications, the radar designer will likely not know or be able to quickly design a two-dimensional function with the analytic properties of AF that can serve as the goal for optimization. Realistically, only a general idea of the desired shape will be known, with the designer seeking to minimize the ambiguity in certain range-Doppler regions.

We introduce the minimization function, denoted as  $M(\tau, u)$ , which serves as the goal for AF optimization. Rather than trying to find an AF which minimizes the MSE between  $M(\tau, u)$  and the synthesized AF  $\chi_x(\tau, u)$ , we are only concerned with ensuring the ambiguity in  $\chi_x$  does not exceed that in the corresponding range-Doppler regions in  $M$ . Consider a possibly complex baseband waveform  $x(t)$  with pulse duration  $T$  seconds, bandwidth  $B$  Hz, and energy  $E$  given by

$$E = \int_{-\infty}^{\infty} |x(t)|^2 dt \quad (17)$$

An  $x(t)$  is desired with AF  $\chi_x(\tau, u)$  having normalized magnitude less than  $M(\tau, u)$  for all range-Doppler combinations which have support, or

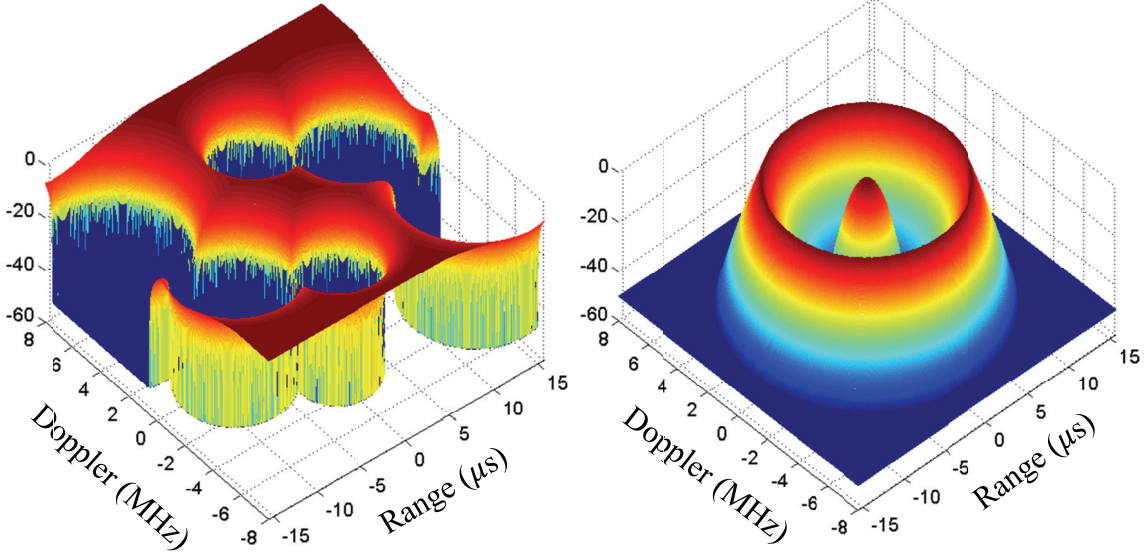


Figure 3: Two examples of possible minimization functions, shown on a decibel (dB) scale. For both plots, Doppler shift is shown on the left axis ( $\pm 8$  MHz) and time delay is shown on the right axis ( $\pm 15$   $\mu$ s).

$$\frac{|\chi_x(\tau, u)|}{|\chi_x(0,0)|} \leq M(\tau, u), \quad \begin{array}{l} -B < u < B \\ -T < \tau < T \end{array} \quad (18)$$

Any two dimensional function which satisfies (18) for a given  $M(\tau, u)$  will be considered a part of the set of minimized functions, denoted as  $\mathcal{M}$ . Shown in Figure 3 are two examples for possible choices for  $M$ .

We will make several main assumptions about the properties of  $M$ . First, we assume that  $M$  is normalized between 0 and 1 and is purely real-valued. This is a valid assumption to make because  $M$  will be compared to the normalized magnitude of  $\chi_x$ , which will also be real-valued between 0 and 1 [1]. Secondly, we assume that the minimization function adheres to the maximum magnitude property of AF [8] [1], where the magnitude of the function is highest at the origin.

$$M_{MAX} = M(0,0) = 1 \geq M(\tau, u), \quad \text{for all } \tau, u \neq 0 \quad (19)$$

Lastly, note that we are only concerned with restricting the magnitude of the AF and no AF generated will have a shape which does not obey the symmetry property [8]:

$$\begin{aligned}\chi^*(-\tau, u) &= \chi(\tau, -u)e^{-2\pi i u \tau} \\ |\chi(-\tau, u)| &= |\chi(\tau, -u)|\end{aligned}\tag{20}$$

Because no AF generated will have a shape which is not axially symmetrical, as shown in (20), and axial symmetry is not a difficult property to impose on our minimization function (we simply build  $M$  for two quadrants and reflect them), we assume that the magnitude of the minimization function will adhere to (20). Note that none of these assumptions are necessarily required when choosing  $M$  for convergence to occur, but choosing an  $M$  with these properties will in most cases allow for quicker and better optimization.

The first projection used will be the projection from the set of AFs  $\mathcal{X}$  to the set of minimized functions  $\mathcal{M}$ . We seek to enforce (18) in the projection, and do so by lowering the magnitude of  $\chi_x$  at range-Doppler combinations where it is not satisfied. The projection,  $P_{\mathcal{M}}$ , is expressed mathematically as

$$\Phi_x(\tau, u) = P_{\mathcal{M}}(\chi_x) = \begin{cases} \chi_x(\tau, u) \frac{M(\tau, u)}{|\chi_x(\tau, u)|}, & (\tau, u) \in \mathcal{B} \\ \chi_x(\tau, u), & (\tau, u) \notin \mathcal{B} \end{cases}\tag{21}$$

where  $\mathcal{B}$  is the set of range-Doppler combinations for which (18) is not satisfied. The result is a possibly complex, two dimensional function for which  $\Phi_x \in \mathcal{M}$ . An example of the projection process is shown in Figure 4. Once we have the minimized function  $\Phi_x$ , an estimate for the waveform whose AF will most closely resemble  $\Phi_x$  must be made.

For this, a projection to the set of temporal waveforms is needed.

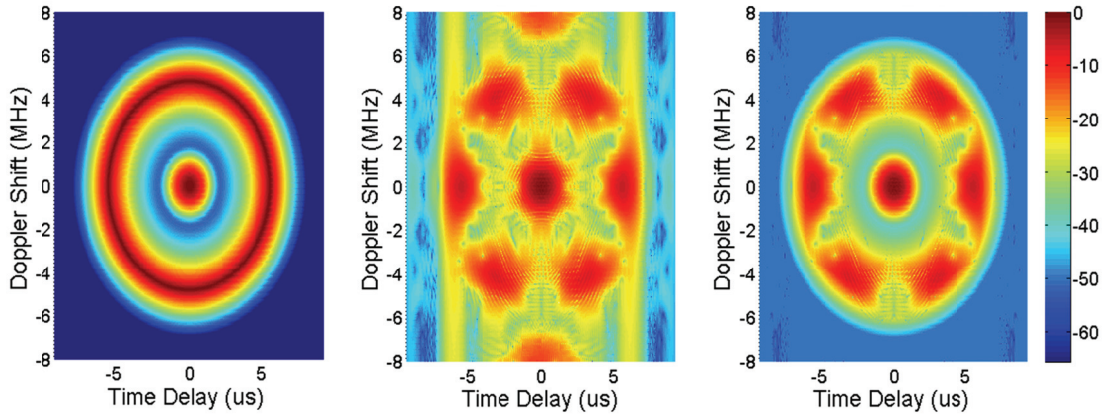


Figure 4: An example of the projection from AF  $\chi_x$  (middle) to minimized function  $\Phi_x$  (right) using minimization function  $M$  (left).

### 3.1.2 Projections to the Time Domain

Let the set of temporal waveforms with pulse duration  $T$  seconds and bandwidth  $B$  Hz be  $\mathcal{S}$ . We seek to project from set  $\mathcal{M}$ , which exists in the two-dimensional range-Doppler space, to set  $\mathcal{S}$ , which exists in the temporal space. When deriving these projections, we first examine some inversions on the AF which accomplish similar goals.

Contrary to its treatment in the literature [1] and radar community, which both indicate that the AF is not invertible, it is possible to invert the AF to find the waveform which generated it [8]. This is assuming we have the AF in its form given in the definition we use;

$$\chi_x(\tau, u) = \int_{-\infty}^{\infty} x(t)x^*(t - \tau)e^{-j2\pi ut} dt, \quad (22)$$

and not just the magnitude definition  $|\chi_x|$  used in some literature [42] [43] [44]. The inversion can be found for both the AF definition in (22) and for the alternate, but equivalent, definition

$$\chi_x(\tau, u) = \int_{-\infty}^{\infty} X(f + u)X^*(f)e^{j2\pi f\tau} df, \quad (23)$$

where  $X(f)$  is the Fourier transform of  $x(t)$

$$X(f) = \mathcal{F}\{x(t)\}$$

The inversion from (22) will first be explored. Note that this equation is an equivalent expression to

$$\chi_x(\tau, u) = \mathcal{F}\{x(t)x^*(t - \tau)\}$$

Taking the inverse Fourier transform gives

$$\mathcal{F}^{-1}\{\chi_x(\tau, u)\} \equiv \int_{-\infty}^{\infty} \chi_x(\tau, u)e^{j2\pi ut} du = x(t)x^*(t - \tau)$$

and setting  $t = 0$  and  $\tau = -\tau$ , we arrive at

$$\int_{-\infty}^{\infty} \chi_x(-\tau, u)du = x(0)x^*(\tau)$$

which can be simplified to the final form of the inversion

$$\mathcal{J}_t(\chi) = \left[ \frac{1}{x(0)} \int_{-\infty}^{\infty} \chi_x(-\tau, u)du \right]^* = x(\tau) \quad (24)$$

where  $\mathcal{J}_t$  is the inversion operator for the above case.

The inversion from (23) can be found in a similar fashion and will now be explored. (23) can be expressed as

$$\chi_x(\tau, u) = \mathcal{F}^{-1}\{X(f + u)X^*(f)\}$$

Taking the Fourier transform gives

$$\mathcal{F}\{\chi_x(\tau, u)\} \equiv \int_{-\infty}^{\infty} \chi_x(\tau, u)e^{-j2\pi f\tau} d\tau = X(f + u)X^*(f)$$

and setting  $f = 0$

$$\int_{-\infty}^{\infty} \chi_x(\tau, u) d\tau = X(u)X^*(0)$$

which can be simplified to the final form of the inversion

$$\mathcal{J}_f(\chi) = \frac{1}{X^*(0)} \int_{-\infty}^{\infty} \chi_x(\tau, u) d\tau = X(u) \quad (25)$$

where  $\mathcal{J}_f$  is the inversion operator for the above case.

The projections used to estimate a waveform from  $\Phi_x$  will be based on the inversions shown in (24), denoted as  $\mathcal{J}_t(\chi)$ , and (25), denoted as  $\mathcal{J}_f(\chi)$ . Note that if  $\chi$  is in the set of AF ( $\chi \in \mathcal{X}$ ), taking the inversion via  $\mathcal{J}_t$  will yield the time domain waveform  $x(\tau)$  corresponding to its uniquely defined Fourier transform  $X(u)$ , produced by taking the inversion via  $\mathcal{J}_f$ . Mathematically, this is expressed as

$$\mathcal{J}_t(\chi) = \mathcal{F}^{-1}\{\mathcal{J}_f(\chi)\} \Leftrightarrow \chi \in \mathcal{X} \quad (26)$$

Additionally, note that that  $\Phi_x \notin \mathcal{X}$  unless the intersection  $\Phi_x \in \mathcal{X} \cap \mathcal{M}$  has been found. This is because  $\Phi_x$  is the projection from  $\mathcal{X}$  to  $\mathcal{M}$ , and the only time a projection doesn't leave the set from which it is being projected when the intersection has been found [38]. Therefore the relationship between the two inversion operations shown in (26) will not usually hold when applying  $\mathcal{J}_t$  and  $\mathcal{J}_f$  to  $\Phi_x$ . For this reason, we use both inversions to form two projections which will be combined to better approximate  $\Phi_x$ . This style of projection is typically used in Generalized Projections, an algorithm based on the same principles as POCS [38], which was discussed in the previous chapter.

The projections are done by applying the inversion principles that were derived and shown in (24) and (25). However, we are not projecting from the set of AFs  $\mathcal{X}$ , but rather from the set of minimized functions  $\mathcal{M}$ . As was previously discussed in the above paragraph, we cannot expect the minimized function  $\Phi_x$  we are now operating on to be in

the set of AF. Therefore, we cannot expect the relationship in (26) to hold, meaning the function we are operating on,  $\Phi_x$ , will not be an AF. As a result, the operations  $\mathcal{J}_t(\Phi_x)$  and  $\mathcal{J}_f(\Phi_x)$  cannot be called inversions, because applying them separately to a function which is not an AF will result in two different time domain functions, as the two only agree when they are operating on a function which is an AF. These operations will still be used, but will be referred to as projections, or

$$y(t) = P_S^t(\Phi_x) = \frac{1}{u(0)} \int_{-B}^B \Phi_x^*(-\tau, u) du \quad (27)$$

$$z(t) = P_S^f(\Phi_x) = \frac{1}{u(0)} \mathcal{F}^{-1} \left\{ \int_{-T}^T \Phi_x(\tau, u) d\tau \right\} \quad (28)$$

where  $u(t)$  is the inversion of the original AF  $\chi_x$ ,

$$u(t) = \mathcal{J}_t(\chi_x) = \mathcal{F}^{-1} \{ \mathcal{J}_f(\chi_x) \}$$

Note that the inverse Fourier transform is taken in (28) to convert the frequency domain projection to a time domain waveform,  $z(t)$ .

Each projection gives different information about  $\Phi_x$ :  $P_S^t(\Phi_x)$  shows the summation along the  $u$  axis, giving information about changes in Doppler, while  $P_S^f(\Phi_x)$  shows the summation along the  $\tau$  axis, giving information about changes in range. Thus, a weighted combination of the two projections is likely to give us more information about how the next candidate waveform needs to be adjusted in both the range and Doppler regions than a single projection could.

We consider two different types of weighting the projections: a minimax weighting and a mean squares weighting. The purpose of having two weighting methods will be further explored when the distance functions are examined, but both are based on the amount of change that occurs in the range or Doppler dimension when projecting

from  $\mathcal{X}$  to  $\mathcal{M}$ . If there is a lot of change in the Doppler summation when compared to the range summation, we can assume that the AF of the waveform needs to be changed more in the frequency domain. On the other hand, if there is a lot of change in the range summation when compared to the Doppler summation, we can assume that the AF of the waveform needs to be changed more in the time domain. Thus, the projection with more change in its respective summation dimension will be weighted higher.

The minimax weighting is determined by the largest difference between the summation in each projection's respective dimension, and is given by the functions

$$\begin{aligned} W_m^t(\Phi_x, \chi_x) &= \max_{\tau} \left| \int_{-B}^B \chi_x(\tau, u) du - \int_{-B}^B \Phi_x(\tau, u) du \right| \\ W_m^f(\Phi_x, \chi_x) &= \max_u \left| \int_{-T}^T \chi_x(\tau, u) d\tau - \int_{-T}^T \Phi_x(\tau, u) d\tau \right| \end{aligned} \quad (29)$$

The mean-squares weighting are determined by the largest MSE between the summation in each projection's respective dimension, and is given by the functions

$$\begin{aligned} W_s^t(\Phi_x, \chi_x) &= \int_{-T}^T \left| \int_{-B}^B \chi_x(\tau, u) du - \int_{-B}^B \Phi_x(\tau, u) du \right|^2 d\tau \\ W_s^f(\Phi_x, \chi_x) &= \int_{-B}^B \left| \int_{-T}^T \chi_x(\tau, u) d\tau - \int_{-T}^T \Phi_x(\tau, u) d\tau \right|^2 du \end{aligned} \quad (30)$$

The weighted combination of  $y(t)$  and  $z(t)$  is then given by

$$x(t) = W^t(\Phi_x, \chi_x) \cdot y(t) + W^f(\Phi_x, \chi_x) \cdot z(t) \quad (31)$$

with the either the minimax or mean-squares weighting functions being used, depending on the type of optimization. Thus, the projection from  $\mathcal{M}$  to  $\mathcal{S}$  is given by

$$x(t) = P_S(\Phi_x, \chi_x) = W^t(\Phi_x, \chi_x) \cdot P_S^t(\Phi_x) + W^f(\Phi_x, \chi_x) \cdot P_S^f(\Phi_x) \quad (32)$$

The algorithm can then be concisely written as

$$\begin{aligned}
1. \quad x_{n+1}(t) &= P_S(P_{\mathcal{M}}(\chi_{x_n}), \chi_{x_n}) \\
2. \quad x_{n+1}(t) &= x_{n+1}(t) \frac{E}{E_{x_{n+1}}}
\end{aligned} \tag{33}$$

where  $E_x$  is the energy of  $x(t)$ .

### 3.2 Distance Functions

In order to assess the quality of the candidate waveform synthesized at each iteration, a distance function must be created to serve as a numerical metric. The distance function is designed with the intent of measuring how well  $\chi_x$  is fitted to  $M$  and is named as such because we are attempting to measure the distance between the current location in the set of AFs,  $\mathcal{X}$ , to the closest point in the set of minimization functions,  $\mathcal{M}$ . The smaller the distance, the better our synthesized AF adheres to the minimization properties we desire. Two types of optimization, with their respective distance functions, are available: minimax and mean-squares optimization. The corresponding weighting functions are used for each optimization type, and the waveform with the lowest corresponding distance function is chosen as the optimum.

The minimax distance function finds the worst case range-Doppler ambiguity and is given by

$$D_m(\chi_x, \Phi_x) = \max_{(\tau, u) \in \mathcal{B}} \frac{|\chi_x(\tau, u)|}{|\chi_x(0, 0)|} - \frac{|\Phi_x(\tau, u)|}{|\Phi_x(0, 0)|} \tag{34}$$

Note that the value of  $D_m$  will always be between 0 and 1, since  $|\Phi_x(\tau, u)|$  will never exceed  $|\chi_x(\tau, u)|$  and the normalized values will never exceed 1 [1].

The mean-square distance function is determined by the MSE between  $\chi_x$  and  $\Phi_x$  and is given by

$$D_s(\chi_x, \Phi_x) = \frac{1}{(4BT)^2} \int_{-T}^T \int_{-B}^B \left( \frac{|\chi_x(\tau, u)|}{|\chi_x(0,0)|} - \frac{|\Phi_x(\tau, u)|}{|\Phi_x(0,0)|} \right)^2 dud\tau \quad (35)$$

Note that the value of  $D_s$  will always be between 0 and the mean of the normalized magnitude of  $\chi_x$ .

At each iteration, the value of  $D_s$  or  $D_m$  is calculated. If the value of the  $n^{th}$  distance function is lower than that of the previous optimum,  $x_n(t)$  is chosen to be the new optimum waveform. The algorithm can continue to iterate while checking for a new optimum waveform at each iteration.

### 3.3 Results and Conclusions

#### 3.3.1 Results

The algorithm was tested in both simulation and with measurements using a Keysight Technologies signal generator and oscilloscope. Results are provided for four trials, each with a different minimization function. Each trial generated a 540 sample waveform in a maximum of 100 iterations with  $T = 16.81 \mu s$  and  $B = 8 MHz$ . The initial AF  $\chi_{x_0}$  was a ones array in all trials. The results are summarized in Table 1. Graphical results for the simulated mean-squares optimization are shown in Figure 5 through Figure 8 while measured results are shown in Figure 9 through Figure 12; the results from the minimax optimization are now shown because the convergence is extremely similar to that of the mean-squares.

Trial I (Figure 5 and Figure 9) shows the resulting AF produced when initialized with a checkerboard style minimization function. The resulting waveform appears almost periodic and fits most of the AF volume into the five squares on the zero-Doppler axis.

Trial II (Figure 6 and Figure 10) shows the result when initialized with a minimization

function consisting of a sharp diagonal crest. The result is a chirp waveform, which fits most of its ambiguity volume into the crest. Trial III (Figure 7 and Figure 11) is initialized with a minimization function which has several circles depressed into the surface. This might be what a practical implementation looks like, with circles with varying sizes placed near the approximated interferers. Trial IV (Figure 8 and Figure 12) shows the result for a minimization function which has a constrained main lobe and an acceptable region for the ambiguity in a box around the main lobe.

TABLE 1: SUMMARY OF RESULTS

Trial	I		II		III		IV	
Optimization Type	MS	MM	MS	MM	MS	MM	MS	MM
Optimum Iteration	16	14	100	11	81	16	100	100
PAPR (dB)	8.425	8.335	1.714	2.356	8.413	8.891	9.149	9.660
Mean-Squares (Simulation)	14.34e-6	15.00e-6	331.9e-6	464.7e-6	0.427e-6	1.952e-6	0.748e-6	1.073e-6
Minimax (Simulation)	0.04983	0.04774	0.39679	0.35103	0.03346	0.02561	0.01829	0.02688
Mean-Squares (Measured)	15.02e-6	15.07e-6	335.0e-6	469.7e-6	0.796e-6	3.181e-6	0.715e-6	0.953e-6
Minimax (Measured)	0.05751	0.05165	0.40037	0.35218	0.03312	0.03226	0.01503	0.02321

However, there are some results in Table 1 which at face value may be unexpected. We see that the optimum iteration for Trials II and III is much lower in minimax optimization as opposed to mean-squares optimization. This would suggest that the minimax-based algorithm is converging much quicker than the mean-squares. However, looking at Figure 13, we see that while convergence is slightly quicker for

minimax, they both stop making large improvements around the same iteration. The mean-squares optimization continues to slightly improve, while the minimax hits a local minimum early on. We see the quality of the AF in both instances doesn't change a significant amount after a certain number of iterations, meaning that any waveform after a certain point would have practically been just as good and the large difference in the optimum iteration number is not nearly as big of a performance difference as it appears.

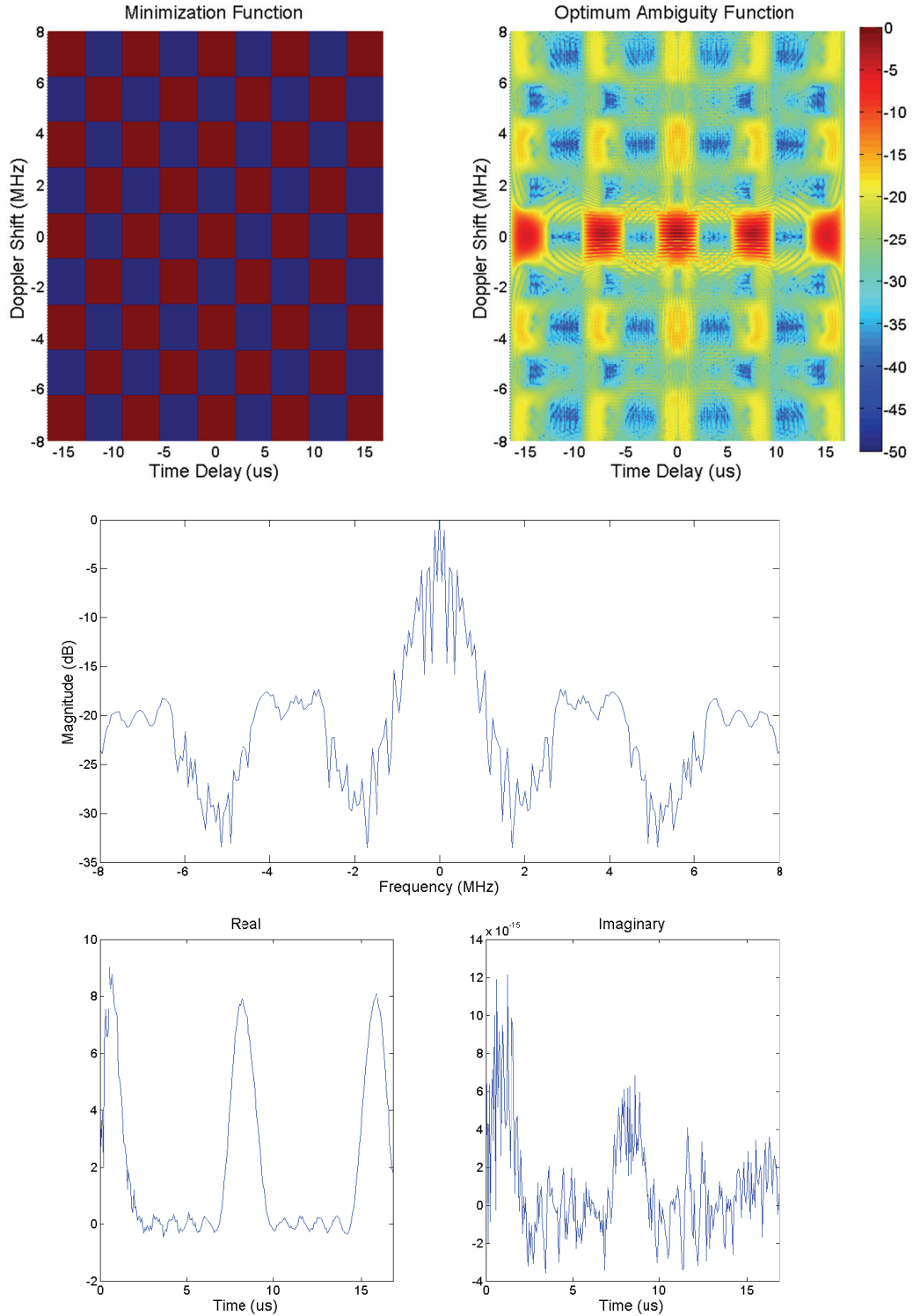


Figure 5: (Simulated) Mean-squares optimization result for trial I. The resulting AF magnitude is compared to the minimization function (top), with the spectrum (middle) and the real and imaginary parts of the time domain (bottom right and left) also displayed.

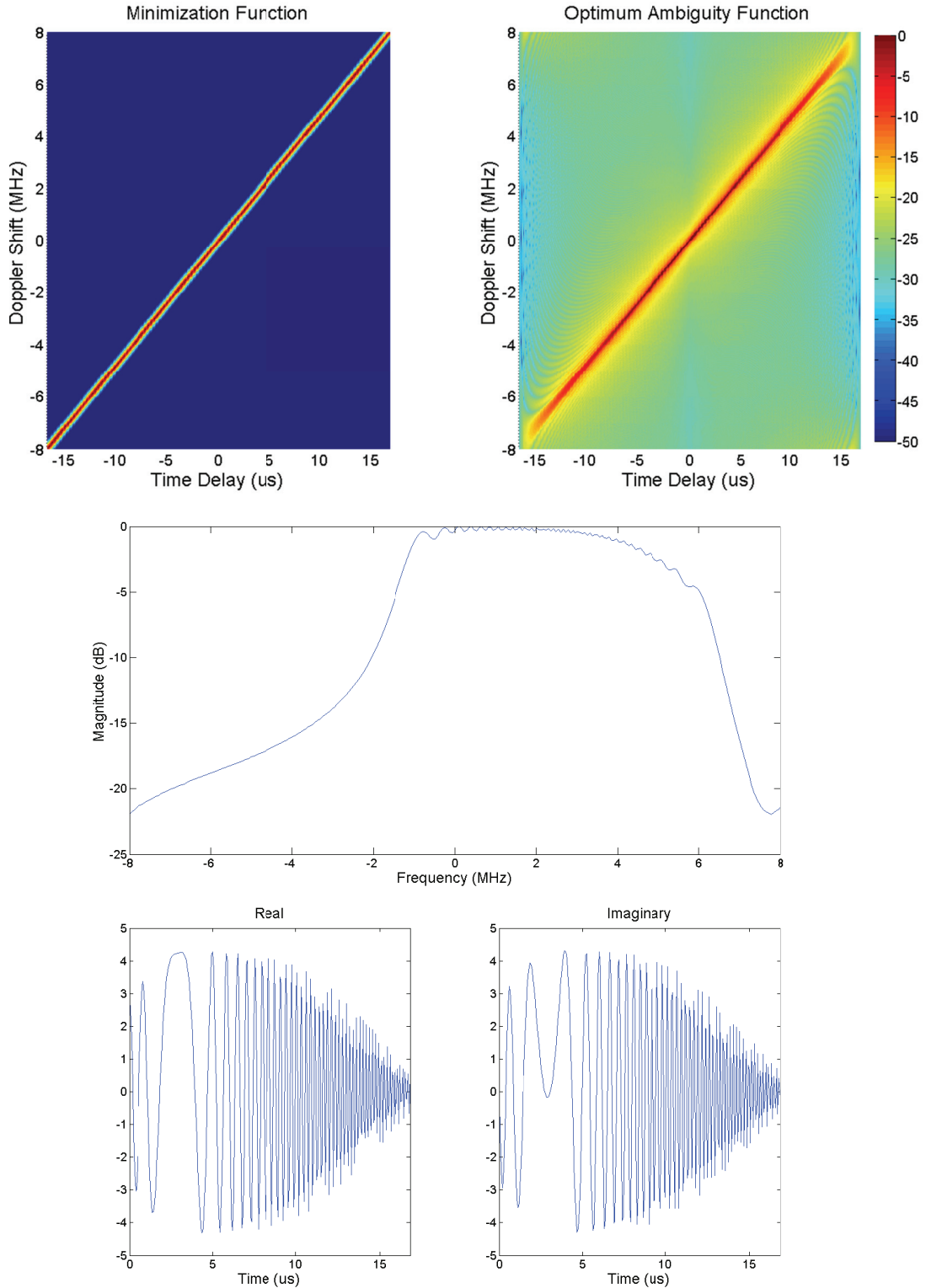


Figure 6: (Simulated) Mean-squares optimization result for trial II. The resulting AF magnitude is compared to the minimization function (top), with the spectrum (middle) and the real and imaginary parts of the time domain (bottom right and left) also displayed.

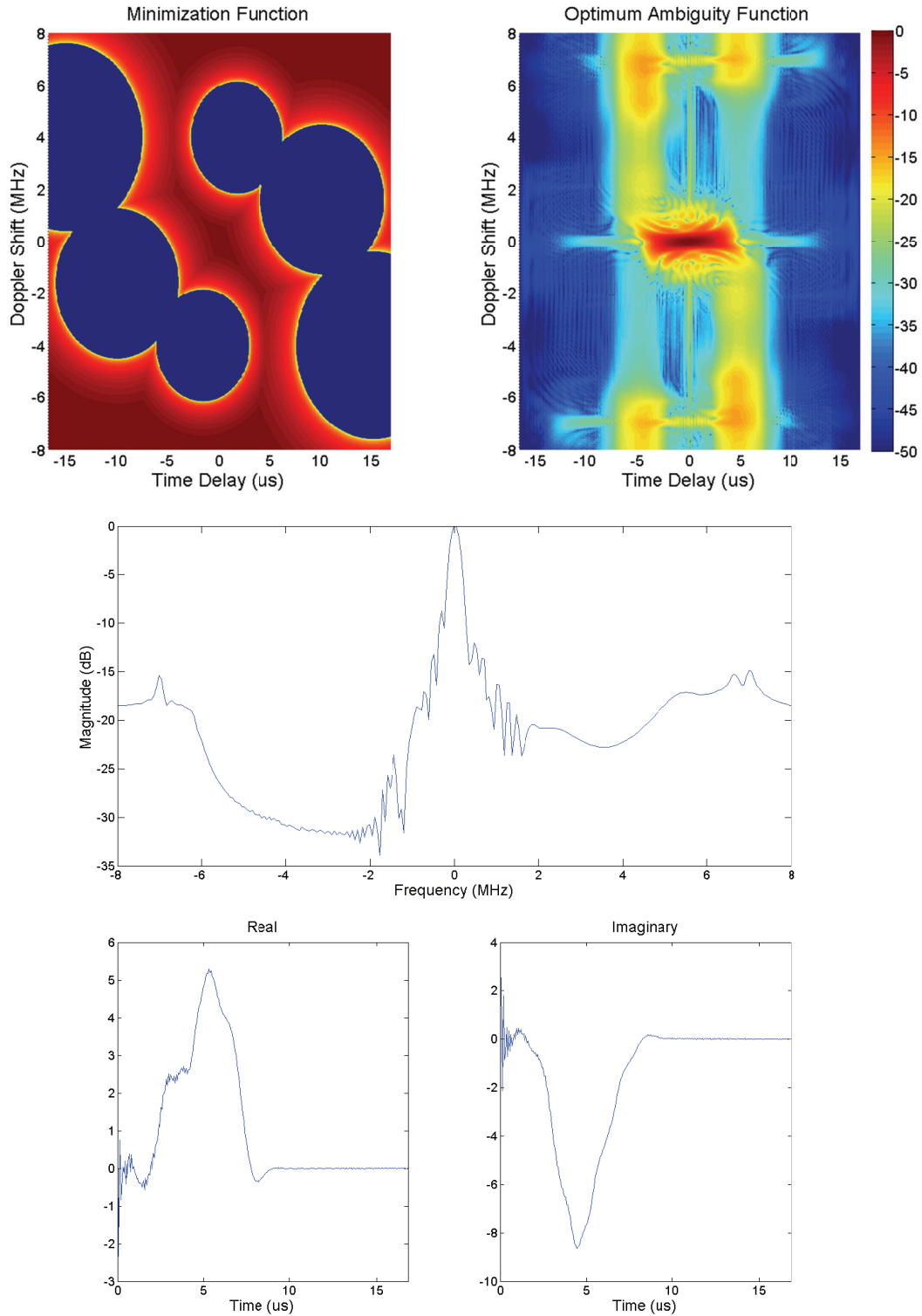


Figure 7: (Simulated) Mean-squares optimization result for trial III. The resulting AF magnitude is compared to the minimization function (top), with the spectrum (middle) and the real and imaginary parts of the time domain (bottom right and left) also displayed.

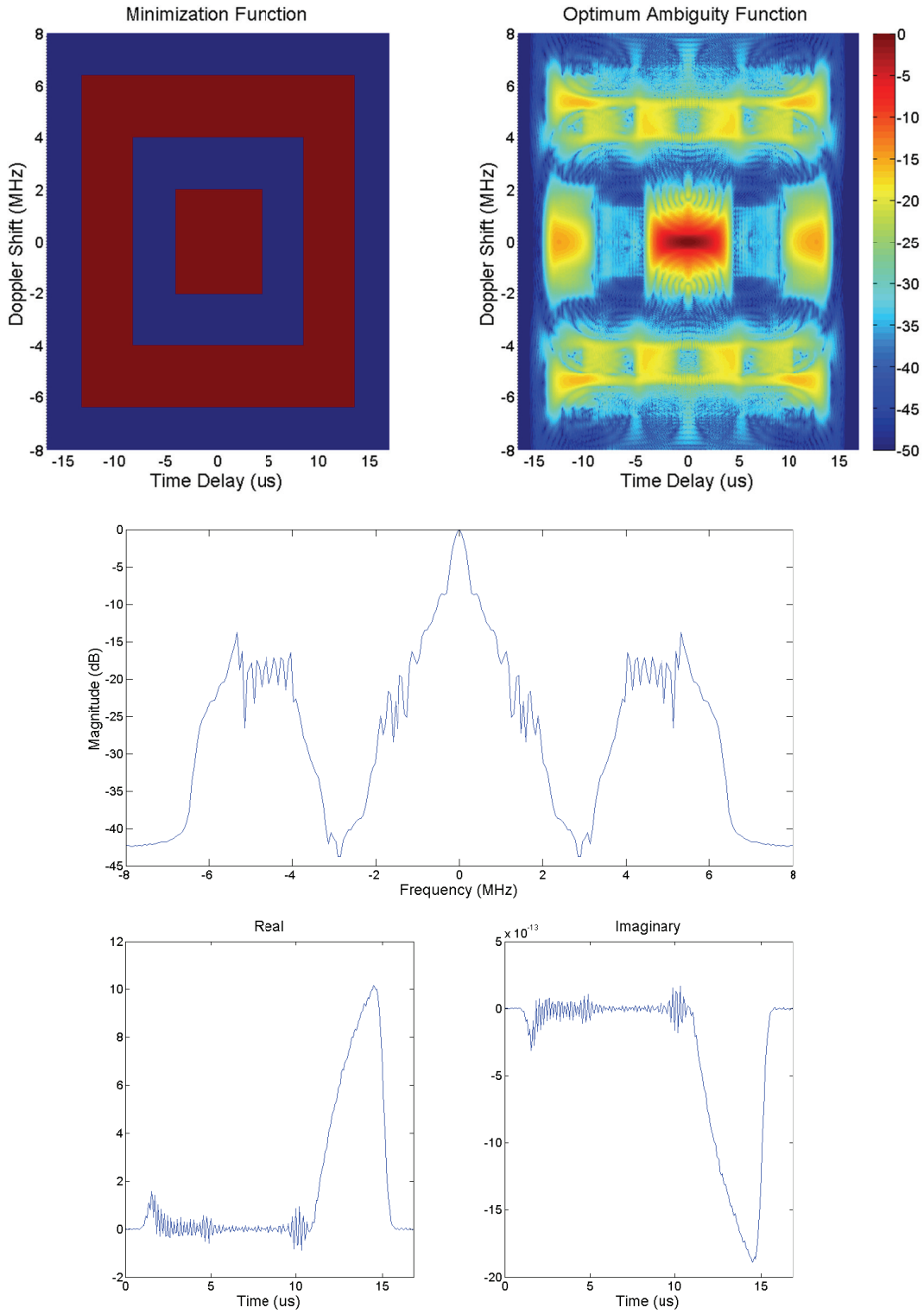


Figure 8: (Simulated) Mean-squares optimization result for trial IV. The resulting AF magnitude is compared to the minimization function (top), with the spectrum (middle) and the real and imaginary parts of the time domain (bottom right and left) also displayed.

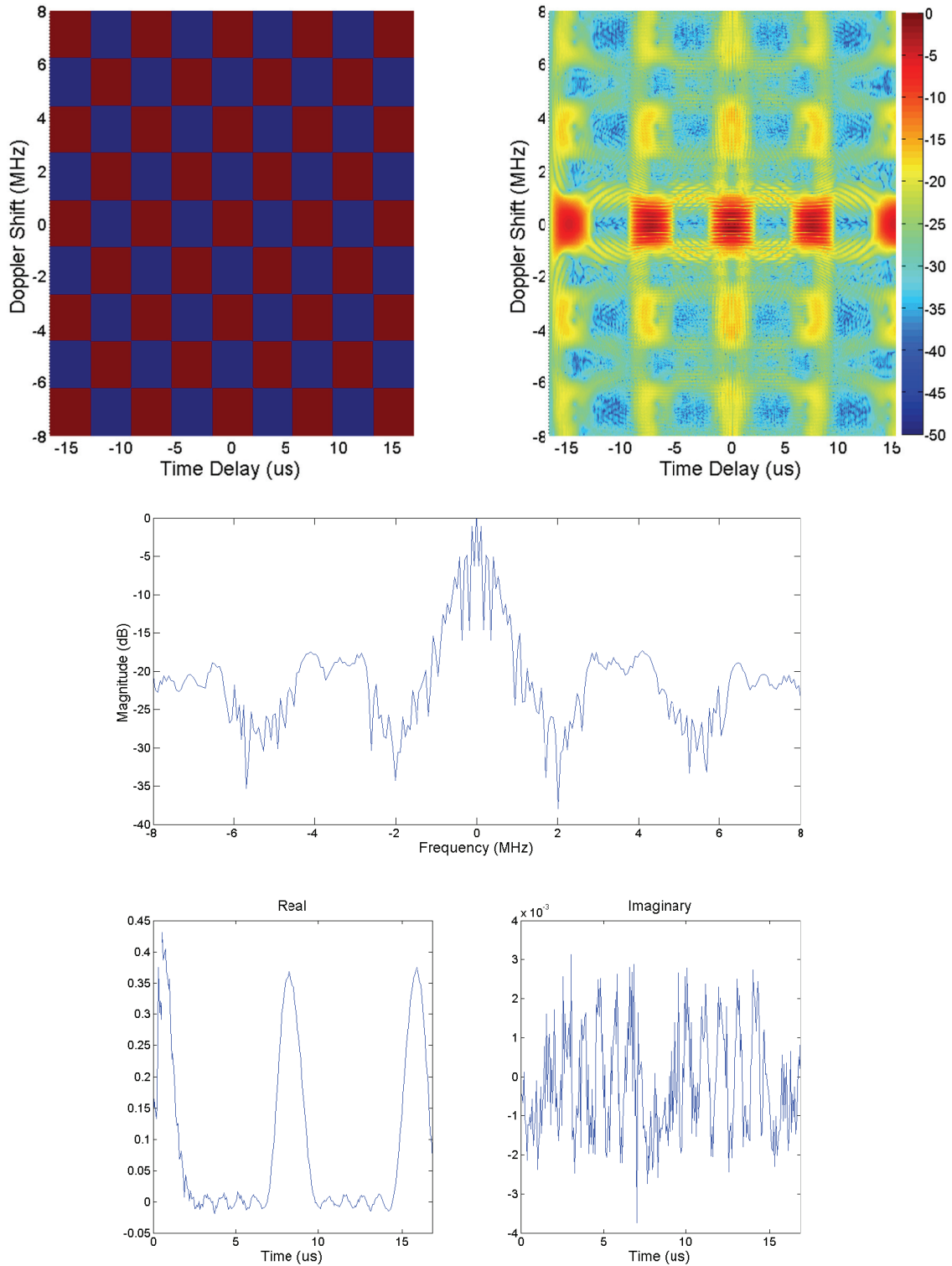


Figure 9: (Measured) Mean-squares optimization result for trial I. The resulting AF magnitude is compared to the minimization function (top), with the spectrum (middle) and the real and imaginary parts of the time domain (bottom right and left) also displayed.

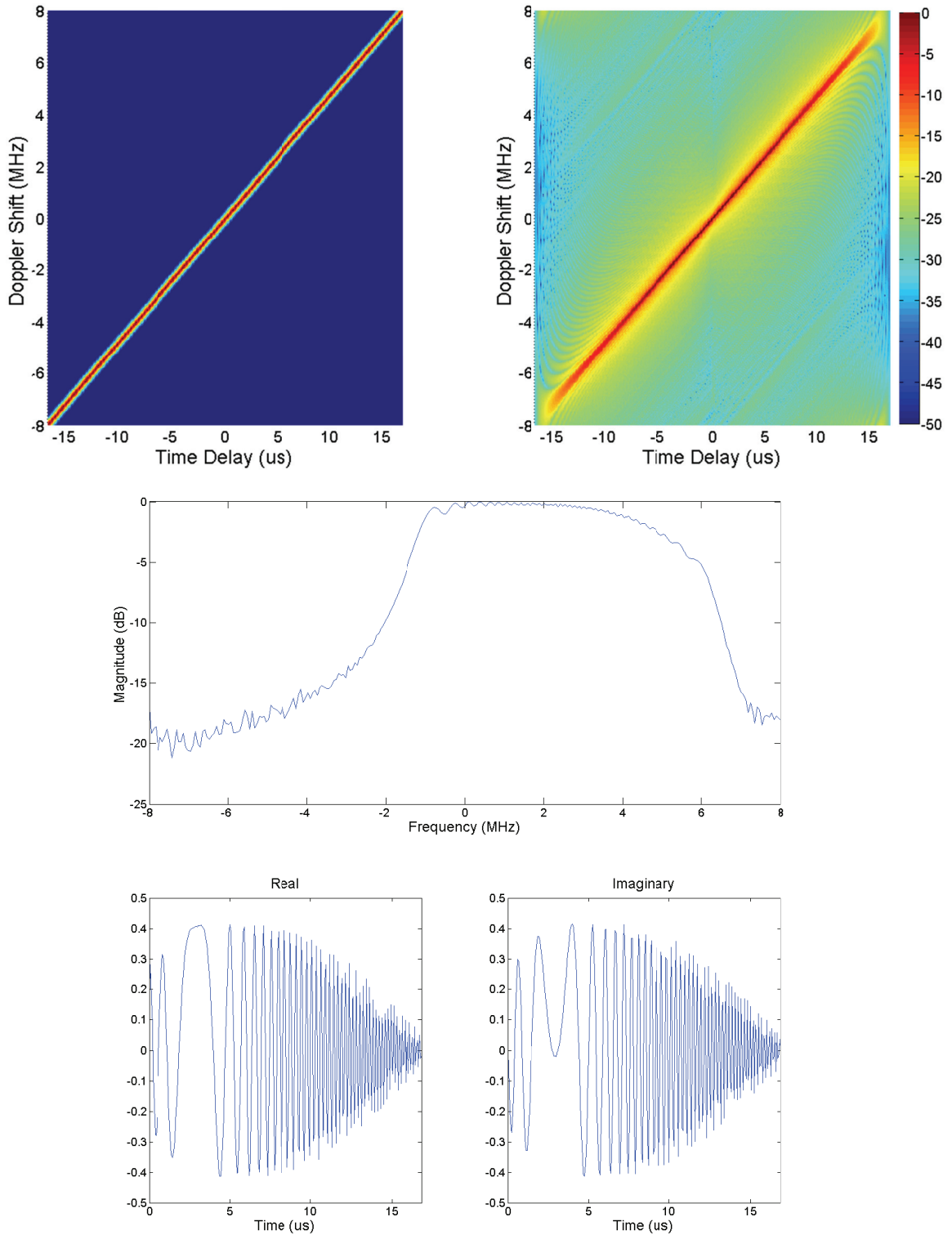


Figure 10: (Measured) Mean-squares optimization result for trial II. The resulting AF magnitude is compared to the minimization function (top), with the spectrum (middle) and the real and imaginary parts of the time domain (bottom right and left) also displayed.

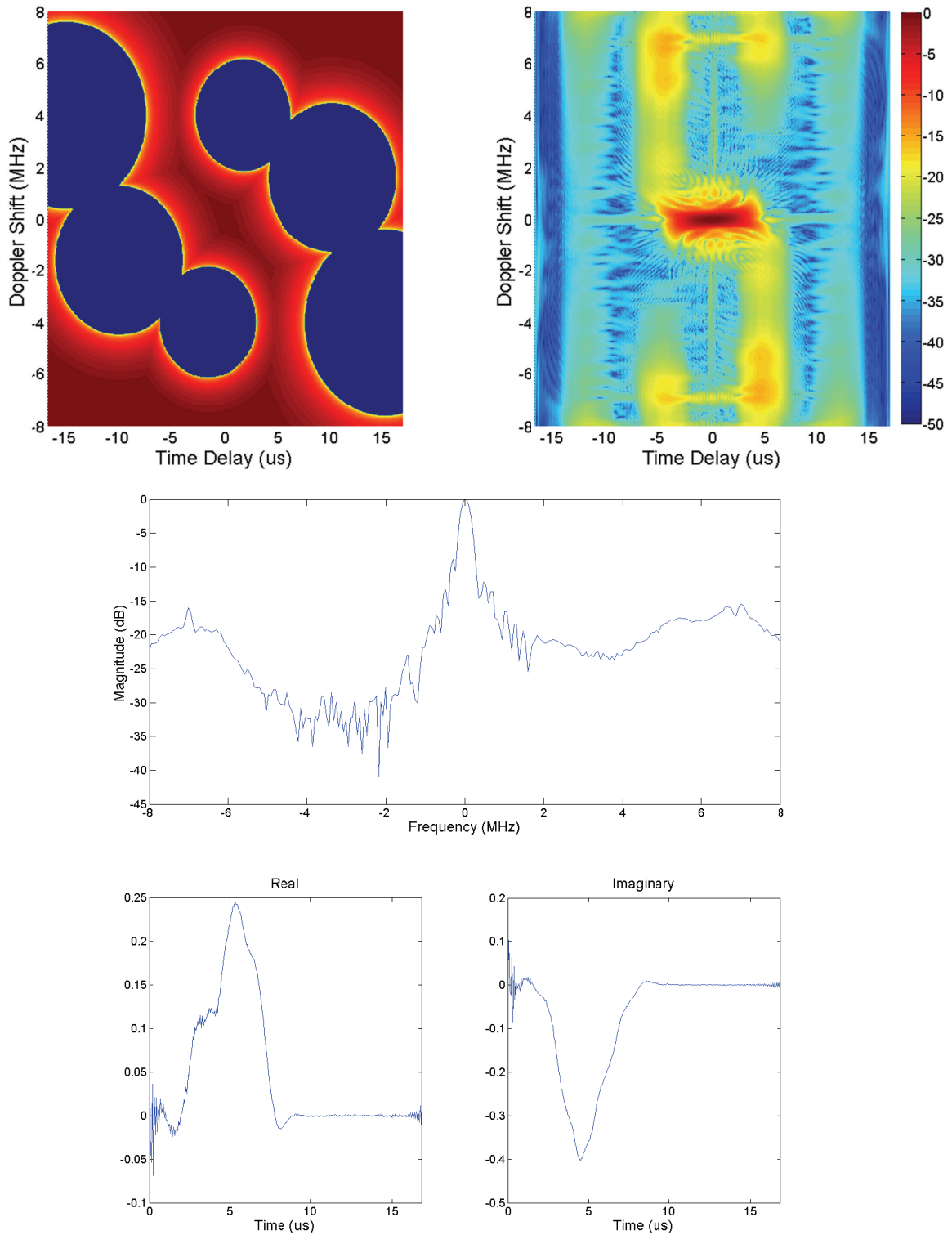


Figure 11: (Measured) Mean-squares optimization result for trial III. The resulting AF magnitude is compared to the minimization function (top), with the spectrum (middle) and the real and imaginary parts of the time domain (bottom right and left) also displayed

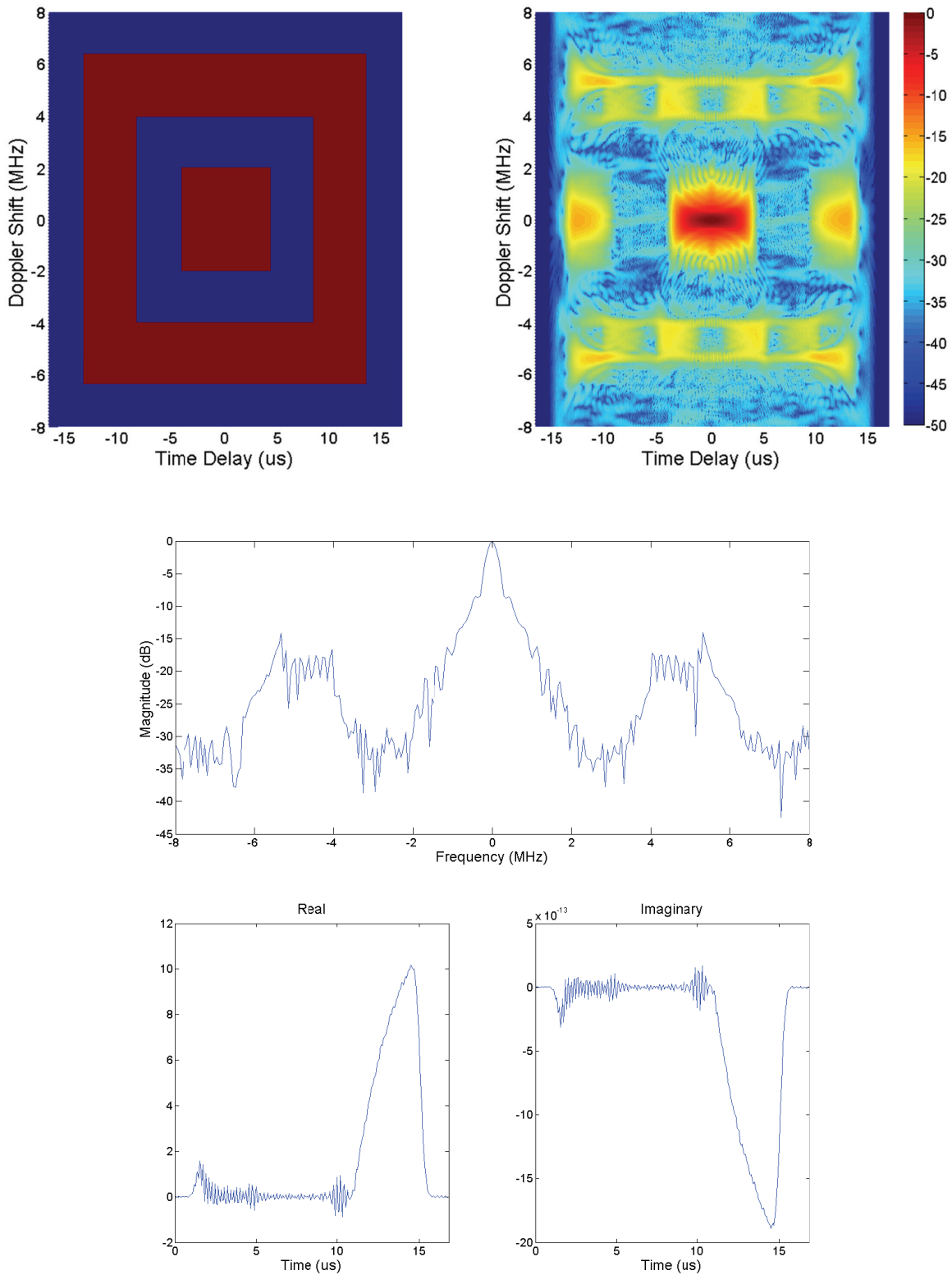


Figure 12: (Measured) Mean-squares optimization result for trial IV. The resulting AF magnitude is compared to the minimization function (top), with the spectrum (middle) and the real and imaginary parts of the time domain (bottom right and left) also displayed.

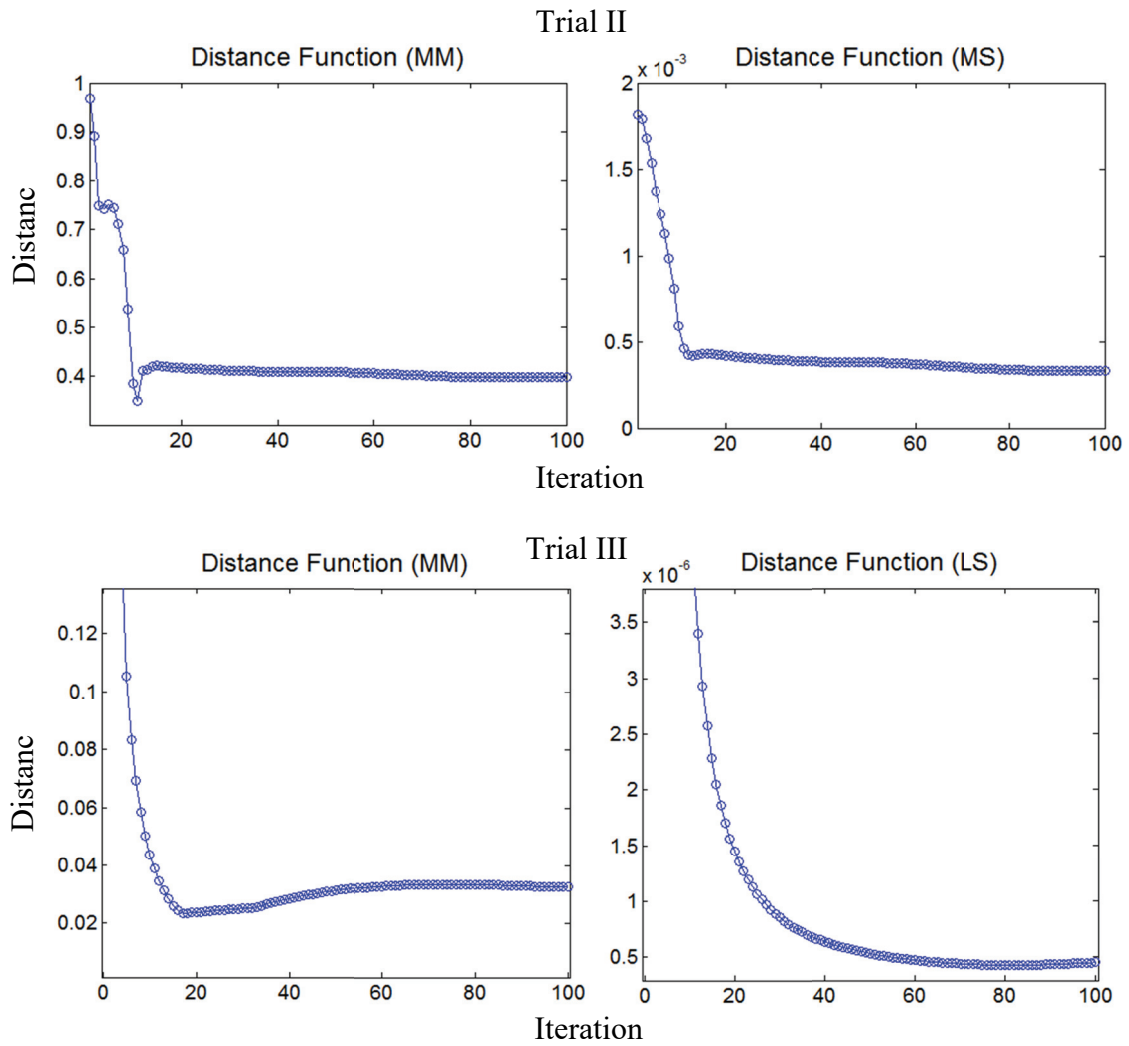


Figure 13: (Simulated) Convergence in Trials II and III for both mean-square and minimax.

### 3.3.2 Conclusions

As seen in the above results, the projections algorithm does a good job of producing waveforms whose AF volume is constrained to regions specified by a chosen minimization function  $M$ . The results shown are expected; the lower magnitude regions of the synthesized AF correspond well with the lower magnitude regions in the minimization function. Additionally, we see the expected implication of minimizing in certain regions: the higher magnitude regions of the synthesized AF correspond with the higher magnitude regions in the minimization function.

An algorithm has been proposed which used alternating projections to dynamically optimize a waveform based on ambiguity minimization criteria in selected range-Doppler regions. Two types of optimization are presented: minimax optimization and mean-squares optimization. Slight variations between the two in the algorithmic process were explained, as well as the differing distance functions used to assess waveform quality. The algorithm is outlined below.

---

Algorithm 1 Waveform synthesis via alternating projections for AF optimization with no external constraints

---

**Input:** Minimization function  $M(\tau, u)$ , initial AF  $\chi_{x_0}(\tau, u)$ , # iterations, optimization type,  $T$ ,  $B$ , desired energy  $E$

**Output:** Optimum waveform  $x_{opt}(t)$

1. **for**  $n = 0 : \# \text{ iterations}$
  2.     **if**  $D(\chi_{x_n}, P_{\mathcal{M}}(\chi_{x_n})) < D_{opt}$
  3.          $D_{opt} = D(\chi_{x_n}, P_{\mathcal{M}}(\chi_{x_n}))$
  4.          $x_{opt}(t) = x_n(t)$
  5.     **end if**
  6.      $x_{n+1}(t) = P_{\mathcal{S}}(P_{\mathcal{M}}(\chi_{x_n}), \chi_{x_n})$
  7.      $x_{n+1}(t) = x_{n+1}(t) \frac{E_{x_n}}{E_{x_{n+1}}}$
  8. **end for**
  9. Return  $x_{opt}(t)$
-

## CHAPTER FOUR

### Designing for Additional Waveform Considerations

In the previous chapter, projections which serve as the basis for our waveform synthesis algorithm were examined. The algorithm outlined was designed to synthesize a waveform  $x(t)$  with pulse duration  $T$  seconds and bandwidth  $B$  Hz with desired ambiguity function (AF) properties. While this approach is very good at designing radar waveforms with an optimized AF, other waveform characteristics must also be considered when designing for radar. This chapter will focus on two very important [45] [7] characteristics: peak-to-average power ratio (PAPR) and the spectrum of the waveform. The PAPR for waveform  $x(t)$  is defined in dB as

$$PAPR = 10 \cdot \log_{10} \left( \frac{|x|_{\text{MAX}}^2}{x_{\text{RMS}}^2} \right) \quad (36)$$

where  $|x|_{\text{MAX}}$  is the maximum magnitude of  $x(t)$ , or

$$|x|_{\text{MAX}} = \operatorname{argmax}_t |x(t)|$$

and  $x_{\text{RMS}}$  is the root-mean square (RMS) value of  $x(t)$  given by

$$x_{\text{RMS}} = \sqrt{\frac{1}{T} \int_0^T |u(t)|^2 dt} \quad (37)$$

The spectrum is defined as the magnitude of the Fourier Transform of  $x(t)$  in the region  $-B \leq f \leq B$  Hz. Section 4.1 will discuss why we are concerned with the PAPR and spectrum of the waveform. Section 4.2.1 will demonstrate how to project onto the set of waveforms with acceptable PAPR, while Section 4.2.2 examines the projection onto the set of waveforms with an acceptable spectrum, and Section 4.2.3 explains how the

projections are combined and fit into the overall algorithm. Section 4.3 gives a brief recap of the algorithm through this chapter, and Section 3.4.2 provides simulation and measurement results using this method.

## *4.1 Considering PAPR and Spectrum*

### *4.1.1 Importance in Waveform Design*

This section will explain why a radar operator would care about a waveform's PAPR and Spectrum, focusing first on PAPR. In order to properly address the importance of PAPR in waveform design, we must first understand some basic operation characteristics of analog RF. There are multiple metrics of measuring the efficiency of a power amplifier [46] [47] [48] [49], including: collector efficiency, overall efficiency, power-added efficiency, and power output capability. These metrics differ slightly and allow us to measure different aspects of an RF power amplifier, but most have a common theme. Increased efficiency is usually associated with increased gain and RF output power, while decreases in efficiency can often be related to increases in DC input power or lower gain. Because of these relationships, a power amplifier will typically be most efficient when operating in the saturation region and will be inefficient when operating over a larger amplitude range or in the linear region. Because operation in the linear region is inefficient and can even have a negative impact on the lifetime of the transmitter [28] [50], lower PAPR can allow operation with increased efficiency of the amplifier.

Due to the increasing number of wireless devices and the United States' National Broadband Plan to convert 500 MHz to broadband wireless communications by 2020, the value of spectrum is currently at an all-time high. While the available spectrum for

civilian and military radar systems is tightening, the importance of these systems mandates the preservation of their accuracy and performance [51]. In addition to using waveforms with lower bandwidth requirements, complications arising from sharing nearby spectral space must also be addressed. A growing area dealing with this is cognitive radio, a technology whose potential implications could allow for great flexibility between devices, resulting in a more efficient use of the spectral space [52]. Cognitive radar has emerged as the use of a similar cognitive approach in radar systems [53] [54]. A waveform synthesis technique which can dynamically adjust its spectrum to allow for coexistence with other wireless devices is of utmost importance when moving towards cognitive radio-friendly technologies. It is well known that non-linearities in power amplifiers result in spectral spreading. One common method of combating this problem in cognitive radio through signal processing is by the use of spectral notching [55], which will be further explored in Section 4.2.2. This work focuses on the use of spectral masks, a measure which is often used in cognitive radio [56] and in wireless transmissions [57] [58].

In short, this chapter will explain methods allowing the waveform we synthesize to be both amplifier and spectrally friendly.

#### *4.2 Projections for PAPR and Spectrum*

Let us again consider possibly complex baseband waveform  $x(t)$ , with pulse duration  $T$  seconds and bandwidth  $B$  Hz. Recall that the set of waveforms with pulse duration  $T$  seconds and bandwidth  $B$  Hz is referred to as  $\mathcal{S}$ . This section will provide the mathematical tools to ensure that  $x(t)$  will also have a user-specified PAPR and energy, as well as a spectrum fitting inside a user-defined spectral mask. Both waveform

characteristics are ensured via a separate alternating projections technique which is computationally inexpensive and will run at the end of each iteration in the main projections algorithm.

#### 4.2.1 Projections to Ensure Desired PAPR

Let the set of waveforms with PAPR less than or equal to  $\Gamma$  be  $\mathcal{P}$  and the set of all waveforms with energy to  $E$  be  $\mathcal{E}$ . Starting from  $x(t) \in \mathcal{E} \cap \mathcal{S}$ , we seek to find an  $x(t)$  which has an acceptable PAPR and energy, or such that

$$x(t) \in \mathcal{S} \cap \mathcal{E} \cap \mathcal{P} \quad (38)$$

It is also useful to note that the intersection between  $\mathcal{E}$  and  $\mathcal{P}$  is non-empty and that a closed form solution for the maximum possible magnitude of a signal existing in the intersection may be easily derived. In other words, consider a signal  $u(t)$  for which (38) is satisfied. The RMS value for  $u(t)$  is first found with (37) and, assuming  $\Gamma$  is given in dB, the calculation for PAPR in (36) is then easily inverted to yield

$$|u|_{\text{MAX}} = u_{\text{RMS}} \sqrt{10^{\frac{1}{10}\Gamma}} = \sqrt{\frac{1}{T} E \cdot 10^{\frac{1}{10}\Gamma}} \quad (39)$$

The set of signals with a maximum magnitude of equal to or less than that given by (39) will be called  $\mathcal{C}$ . This means that, given a desired PAPR  $\Gamma$  and energy  $E$ , we can calculate the maximum acceptable value of the waveform. This value will be referred to as

$$A_c = \sqrt{\frac{1}{T} E \cdot 10^{\frac{1}{10}\Gamma}} \quad (40)$$

Note that because any weighted combination of any two signals with an acceptable PAPR will also have an acceptable PAPR,  $\mathcal{C}$  is a convex set. Additionally the intersection of

waveforms with acceptable energy and maximum magnitude will be a subset of the set of waveforms with acceptable PAPR, or

$$\mathcal{E} \cap \mathcal{C} \subset \mathcal{P} \quad (41)$$

This means that once the intersection of  $\mathcal{E}$  and  $\mathcal{C}$  has been found, (38) is satisfied and a solution has been found.

Because  $\mathcal{C}$  is extremely easy to project to and is convex, it will be used as the set onto which we project from  $\mathcal{E}$  instead of projecting directly to  $\mathcal{P}$ . This projection is done by limiting the maximum magnitude of the waveform to the magnitude calculated by (40), mathematically expressed as

$$x_{\mathcal{C}}(t) = P_{\mathcal{C}}(x) = \begin{cases} x(t) \frac{A_{\mathcal{C}}}{|x(t)|}, & |x(t)| > |x|_{\text{MAX}} \\ x(t), & |x(t)| \leq |x|_{\text{MAX}} \end{cases} \quad (42)$$

The projection back to  $\mathcal{E}$  is done via a simple energy normalization

$$x_{\mathcal{E}}(t) = P_{\mathcal{E}}(x) = x(t) \frac{E}{\int_0^T |x(t)|^2 dt} \quad (43)$$

These projections are applied alternately until the intersection has been found. The algorithm to find a waveform which satisfies (38) can then be written concisely as

$$x_{n+1}(t) = P_{\mathcal{E}}\left(P_{\mathcal{C}}(x_n(t))\right) \quad (44)$$

#### 4.2.2 Projections to Ensure Desired Spectrum

The spectral projection is done in a manner very similar manner to the PAPR projections. Denote the set of all signals whose spectral magnitude falls under a given spectral mask,  $S_m(f)$ , as  $\mathcal{Z}$ . An examples of a spectra which do and do not comply with a given spectral mask are shown in Figure 14. Note that because any weighted combination of any two signals with an acceptable spectrum will also have an acceptable spectrum,  $\mathcal{Z}$

is a convex set. We seek to find a waveform  $x(t)$  which has an acceptable spectrum and energy, or such that

$$x(t) \in \mathcal{S} \cap \mathcal{E} \cap \mathcal{Z} \quad (45)$$

An example of spectra which do and do not comply with a spectral mask are shown in

$$x_{n+1}(t) = P_{\mathcal{E}}\left(P_{\mathcal{Z}}(x_n(t))\right) \quad (46)$$

To project onto  $\mathcal{Z}$ , we simply lower the magnitude at frequencies where it exceeds the user-defined spectral mask, which is shown mathematically by

$$x_{\mathcal{Z}}(t) = \mathcal{F}^{-1}\{P_{\mathcal{Z}}(x)\} = \begin{cases} \frac{S_m(f)}{\beta}, & |\mathcal{F}\{x(t)\}| > S_m(f) \\ \mathcal{F}\{x(t)\}, & |\mathcal{F}\{x(t)\}| \leq S_m(f) \end{cases} \quad (47)$$

where  $\beta$  is the user-defined optional padding factor. Note that this projection will lower the energy of the waveform if  $x(t) \notin \mathcal{E} \cap \mathcal{Z}$  before the projection. To account for the decrease in energy the projection shown in (43) is done. These two projections alternate until a waveform satisfying (45) is found. The algorithm to find a waveform which satisfies (45) can then be written concisely as

$$x_{n+1}(t) = P_{\mathcal{Z}}\left(P_{\mathcal{E}}(x_n(t))\right) \quad (48)$$

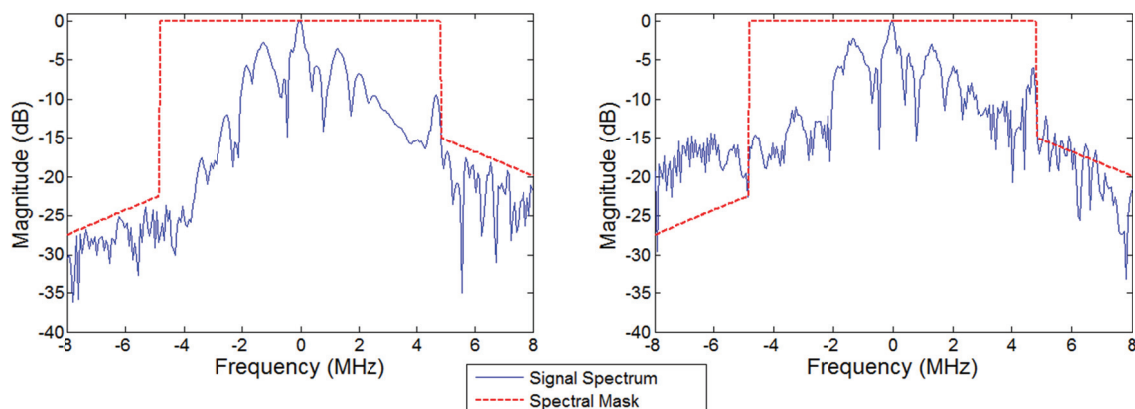


Figure 14: An example of a spectrum which is compliant with a spectral mask (left) and one which is not (right)

One interesting aspect of the method used to ensure spectral compliance is that it only depends on the shape of the desired spectral magnitude. An implication of this is that useful waveform characteristics, such as spectrum notching, can be easily implemented by altering  $S_m$ . An example of a notched waveform created using this method is shown in Figure 15.

#### 4.2.3 Ensuring Both Desired Spectrum and Desired PAPR

The previous two subsections discussed methods which ensure that the synthesized waveform will have a desired PAPR and spectrum, respectively. Building off of these methods, we can easily combine the projections to jointly ensure both criteria are met. We find a waveform with acceptable PAPR, spectrum, and energy, such that

$$x(t) \in \mathcal{S} \cap \mathcal{E} \cap \mathcal{P} \cap \mathcal{Z} \quad (49)$$

with an alternating projections algorithm based on the previous projections, written as

$$x_{n+1}(t) = P_c \left( P_\varepsilon \left( P_Z \left( x_n(t) \right) \right) \right) \quad (50)$$

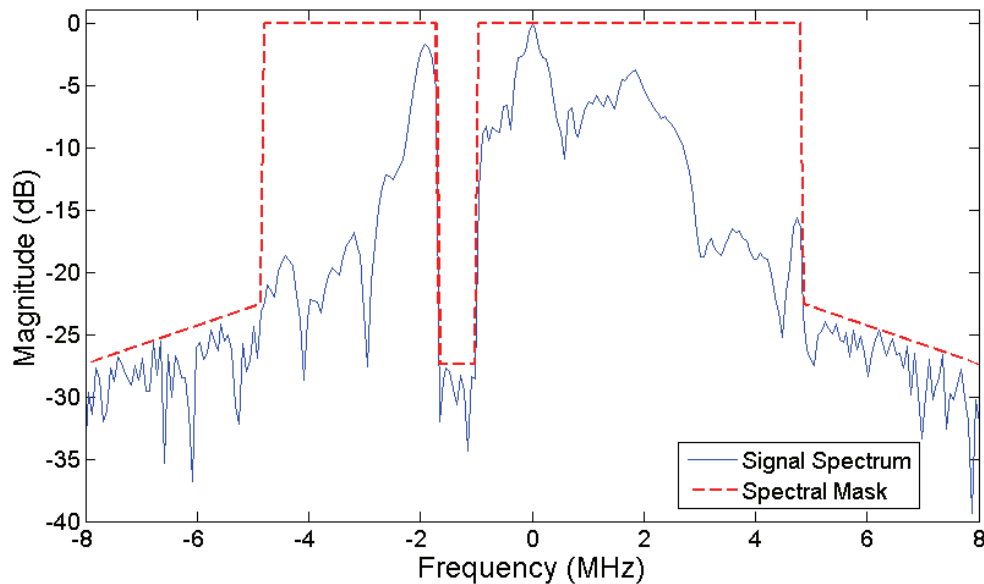


Figure 15: Spectrum of a notched waveform created using the projections algorithm

which iterates until either (49) is satisfied or adequately near.

### 4.3 Results and Conclusions

#### 4.3.1 Results

The algorithm is tested in both simulation and with measurements using a Keysight Technologies signal generator and oscilloscope. Results are provided for four trials, each with a different minimization function. Each trial generated a 540 sample waveform in a maximum of 100 iterations with  $T = 16.81 \mu s$  and  $B = 8 MHz$ . The initial AF  $\chi_{x_0}$  was a ones array in all trials. The maximum allowed PAPR is 2 dB in all trials and the spectral mask is shown in red in the middle figure of the spectrum on each page. The results are summarized in Table 2. Graphical results for the simulated mean-squares optimization are shown in Figure 16 through Figure 19 while measured results are shown in Figure 20 through Figure 23. The results for minimax optimization are not shown, as their convergence is graphically very similar to that of the mean-squares optimization.

Trial I (Figure 16 and Figure 20) shows the resulting AF produced when initialized with a checkerboard style minimization function. The resulting waveform appears almost periodic and fits most of the AF volume into the five squares on the zero-Doppler axis. Trial II (Figure 17 and Figure 21) shows the result when initialized with a minimization function consisting of a sharp diagonal crest. The result is a chirp waveform, which fits most of its ambiguity volume into the crest. Trial III (Figure 18 and Figure 22) is initialized with a minimization function which has several circles depressed into the surface. This might be what a practical implementation looks like, with circles

with varying sizes placed near the approximated interferers. Trial IV (Figure 19 and Figure 23) shows the result for a minimization function which has a constrained main lobe and an acceptable region for the ambiguity in a box around the main lobe.

TABLE 2: SUMMARY OF RESULTS

Trial	I		II		III		IV	
	MS	MM	MS	MM	MS	MM	MS	MM
Desired Energy	3400	3400	3400	3400	3400	3400	3400	3400
Desired PAPR	2 dB							
PAPR (dB)	1.9998	1.9998	1.4734	1.9999	2.0000	1.9996	1.9999	1.9999
Optimum Iteration	100	43	89	100	53	61	15	20
Mean-Squares (Simulation)	240.0e-6	260.3e-6	275.8e-6	511.9e-6	147.4e-6	215.9e-6	205.9e-6	208.5e-6
Minimax (Simulation)	0.23994	0.22426	0.36475	0.43895	0.16660	0.14282	0.24662	0.14560
Mean-Squares (Measured)	236.6e-6	255.7e-6	276.0e-6	515.0e-6	146.0e-6	212.9e-6	190.8e-6	185.4e-6
Minimax (Measured)	0.24195	0.22239	0.37018	0.44106	0.16621	0.14128	0.25200	0.13660

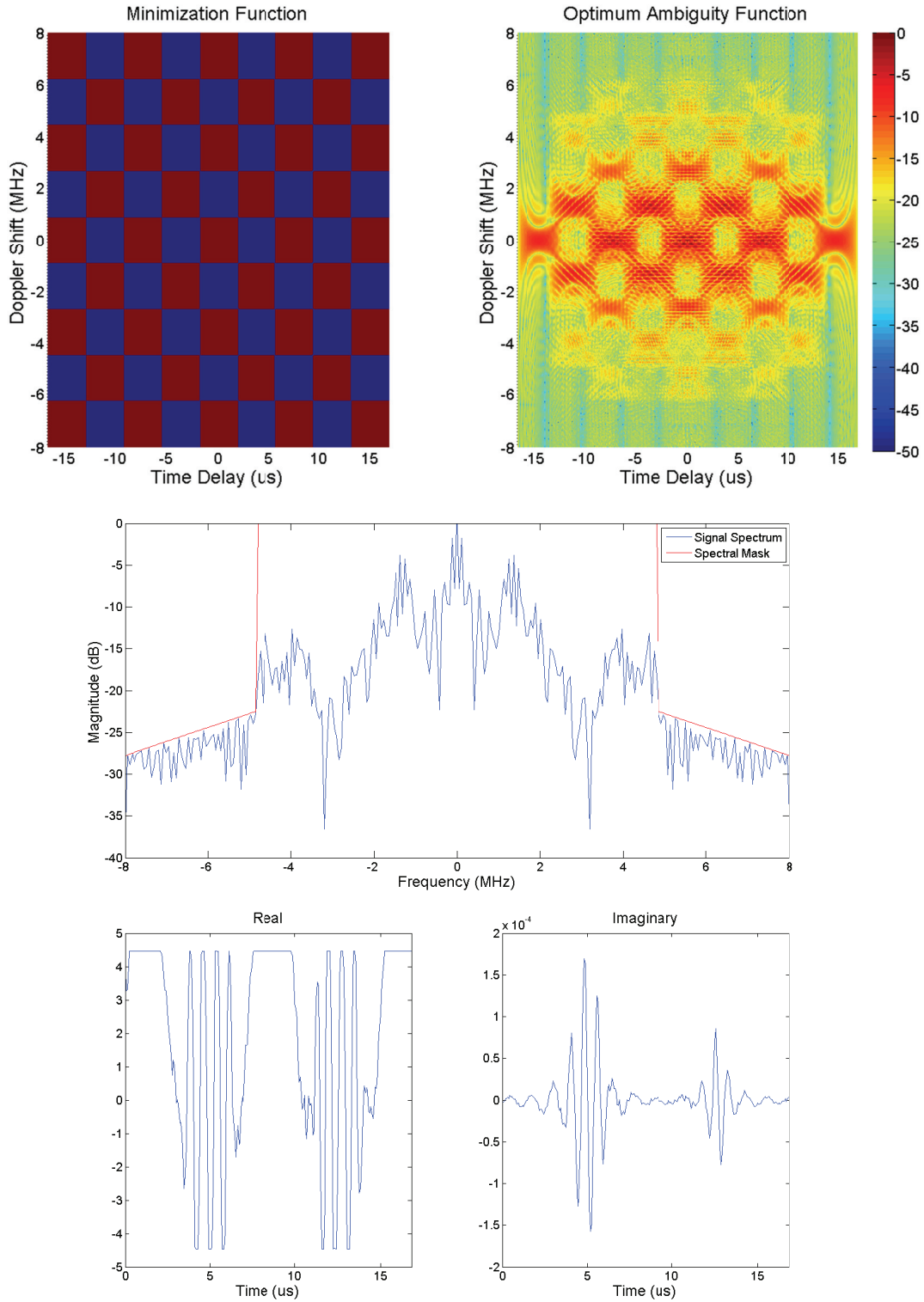


Figure 16: (Simulated) Mean-squares optimization result for trial I. The resulting AF magnitude is compared to the minimization function (top), with the spectrum (middle, includes mask) and the real and imaginary parts of the time domain (bottom right and left) also displayed.

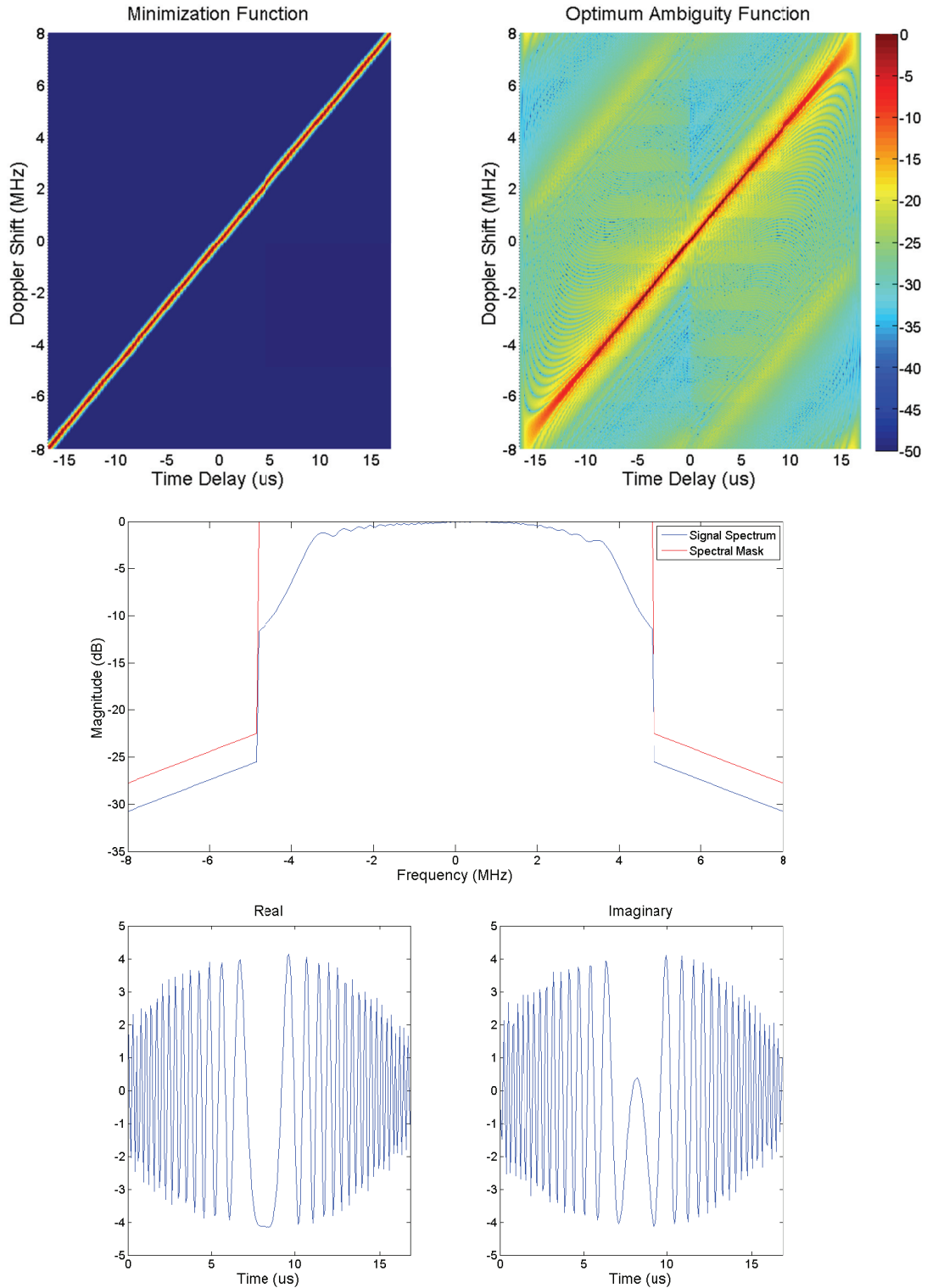


Figure 17: (Simulated) Mean-squares optimization result for trial II. The resulting AF magnitude is compared to the minimization function (top), with the spectrum (middle, includes mask) and the real and imaginary parts of the time domain (bottom right and left) also displayed.

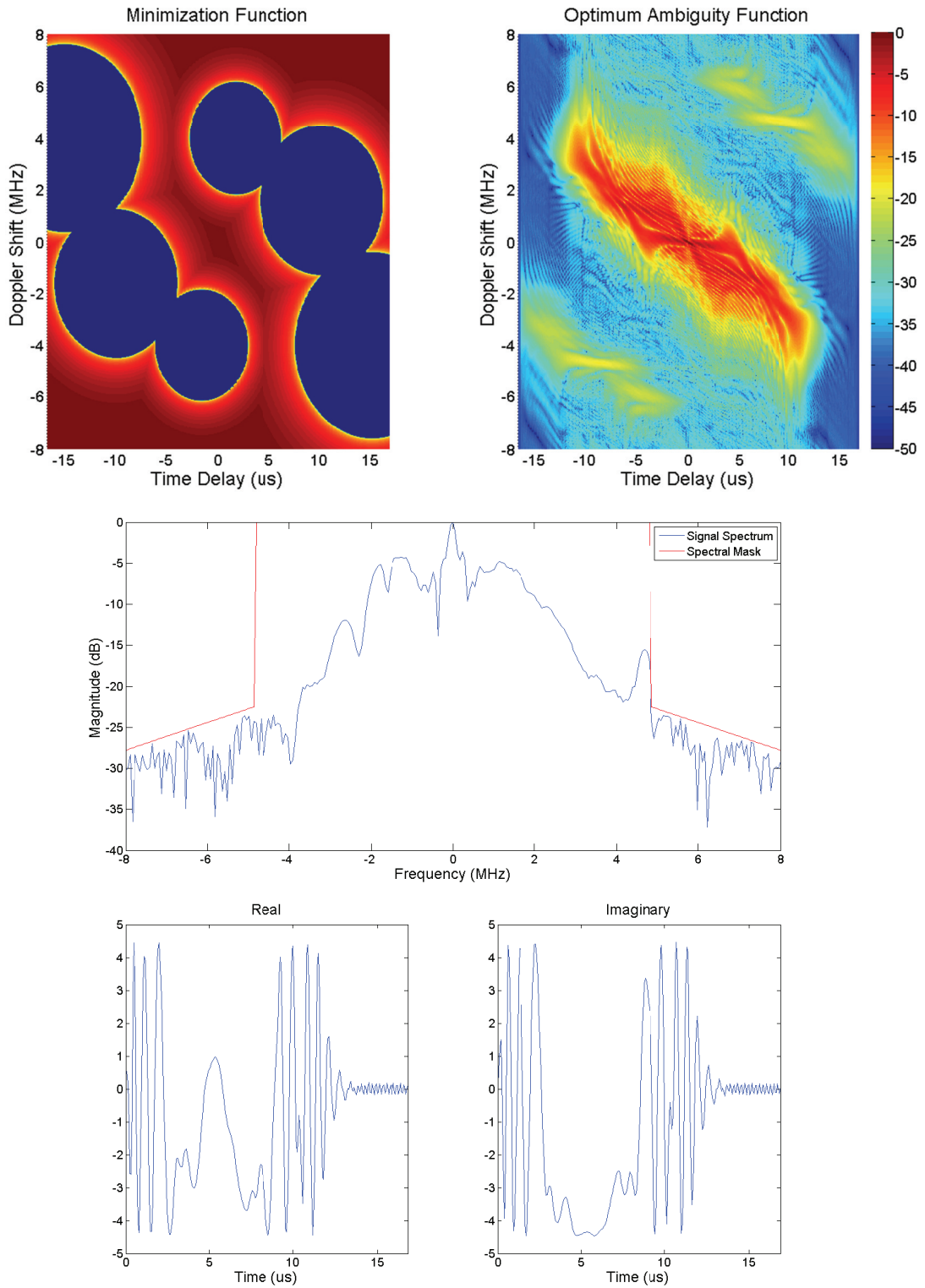


Figure 18: (Simulated) Mean-squares optimization result for trial III. The resulting AF magnitude is compared to the minimization function (top), with the spectrum (middle, includes mask) and the real and imaginary parts of the time domain (bottom right and left) also displayed.

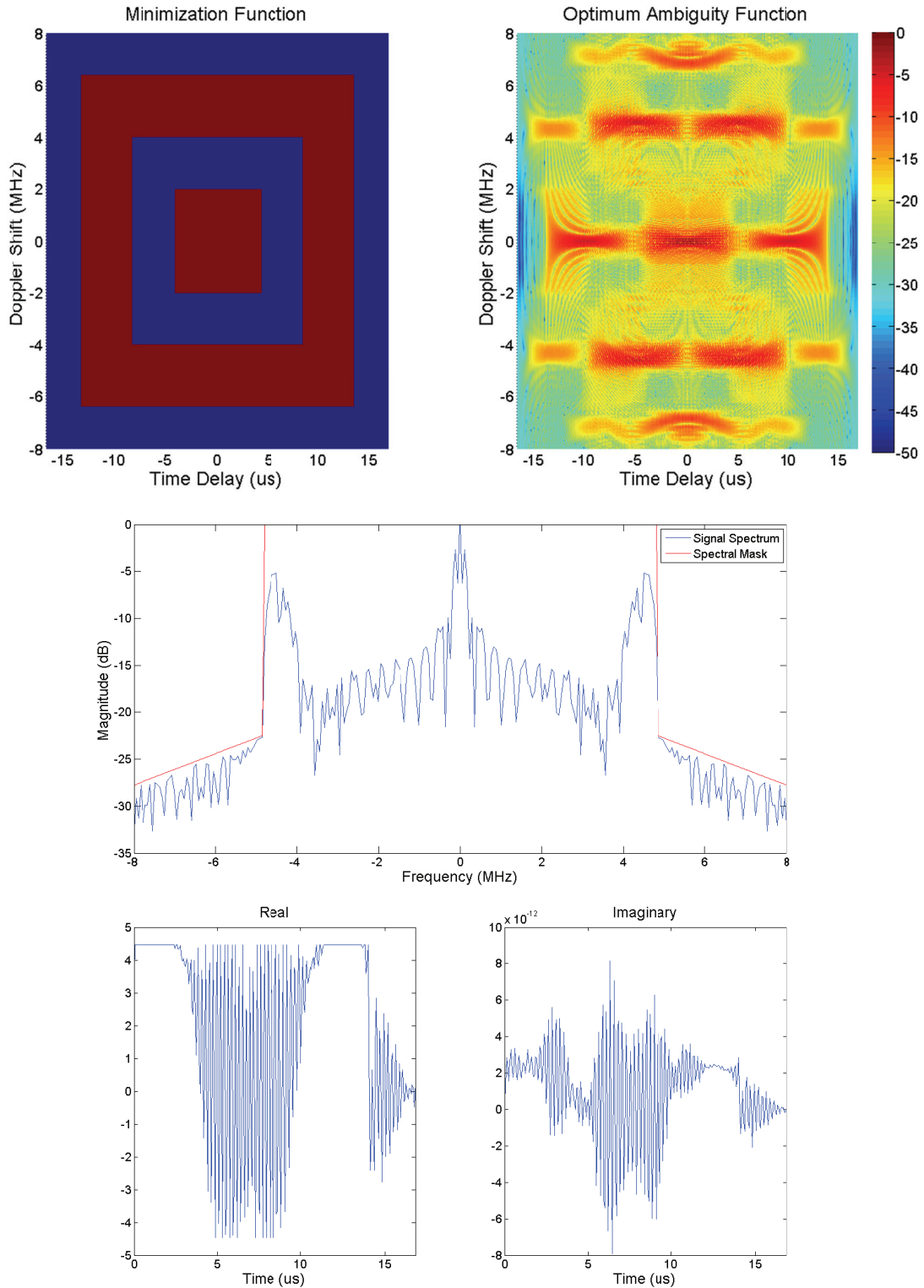


Figure 19: (Simulated) Mean-squares optimization result for trial IV. The resulting AF magnitude is compared to the minimization function (top), with the spectrum (middle, includes mask) and the real and imaginary parts of the time domain (bottom right and left) also displayed.

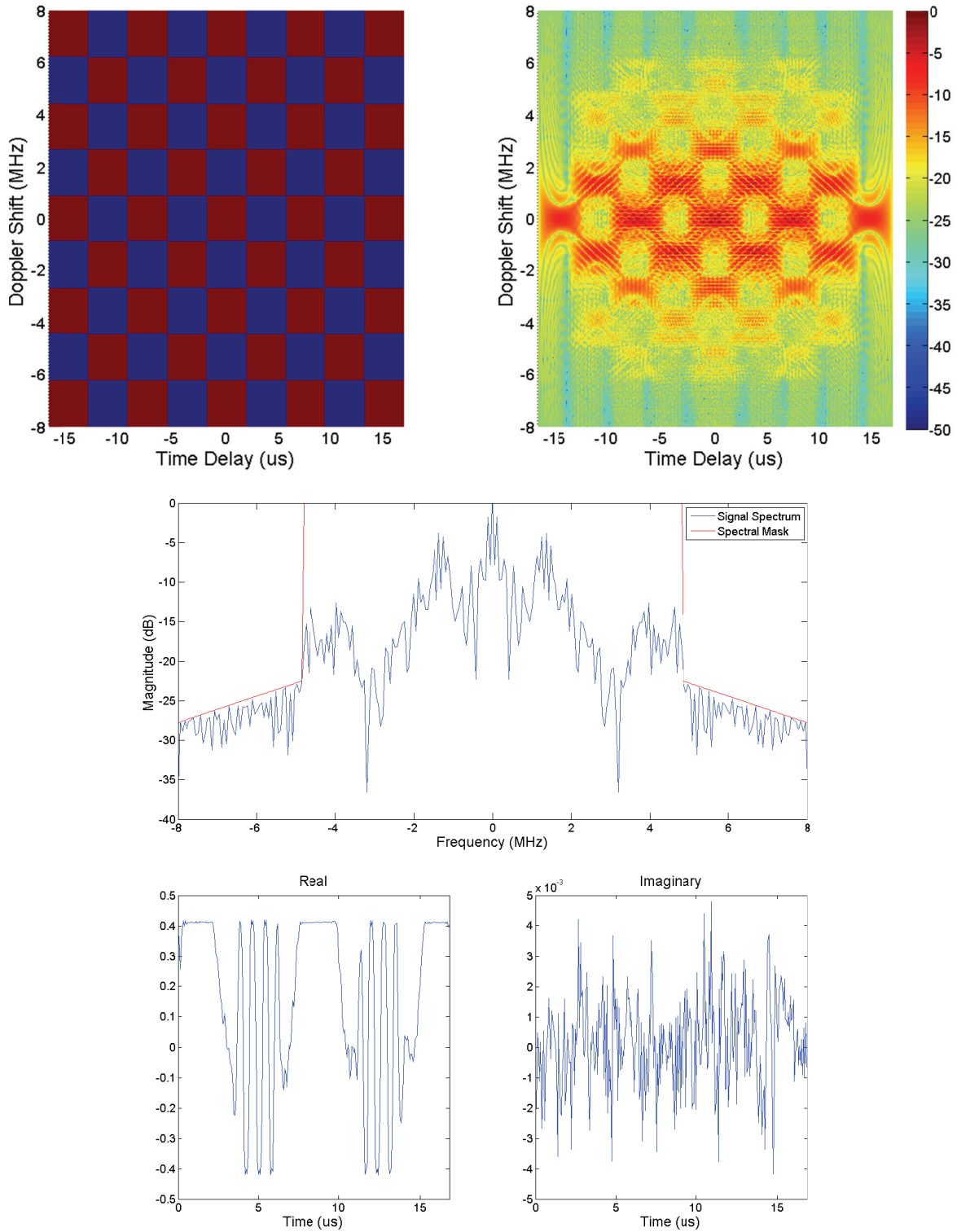


Figure 20: (Measured) Mean-squares optimization result for trial I. The resulting AF magnitude is compared to the minimization function (top), with the spectrum (middle, includes mask) and the real and imaginary parts of the time domain (bottom right and left) also displayed.

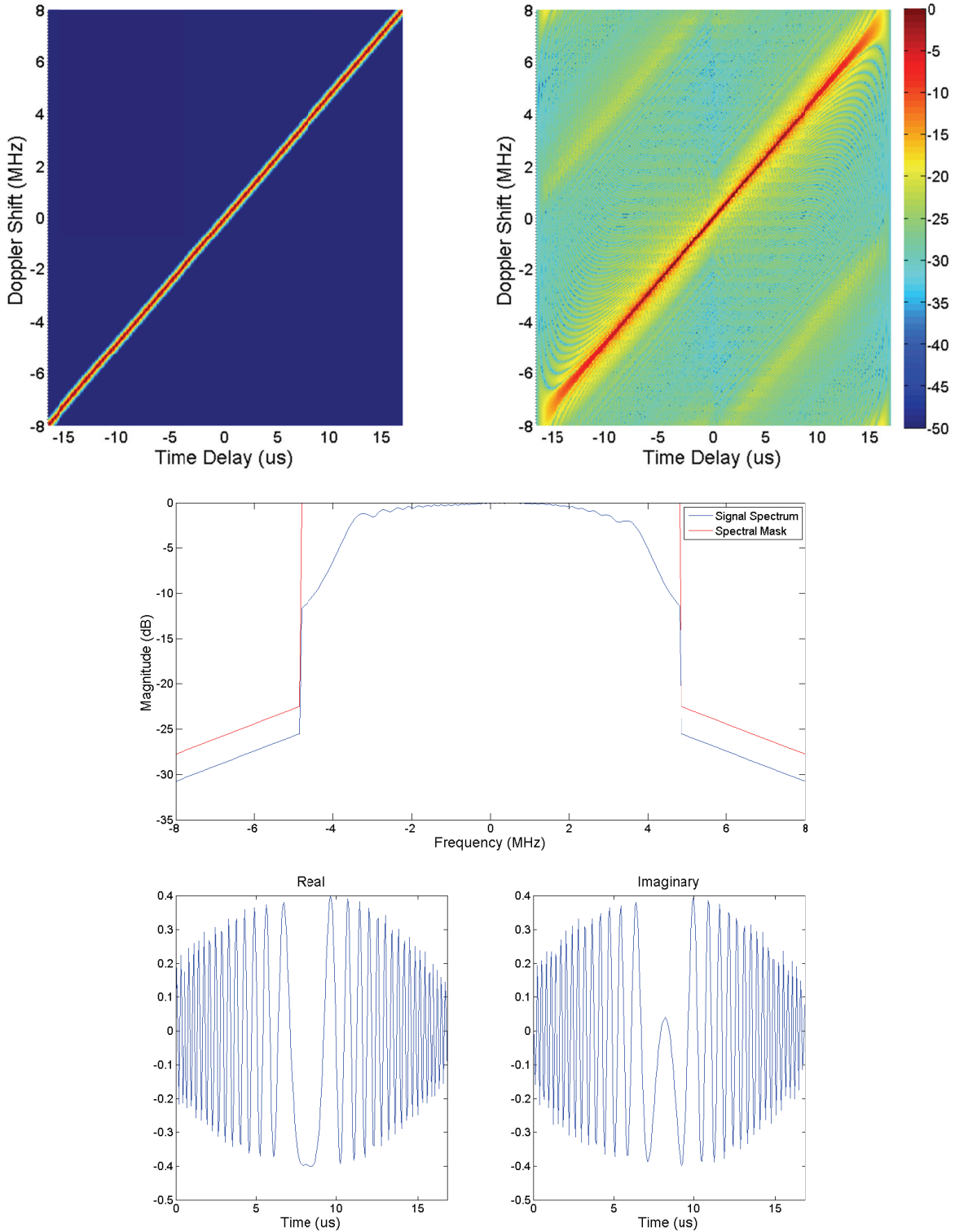


Figure 21: (Measured) Mean-squares optimization result for trial II. The resulting AF magnitude is compared to the minimization function (top), with the spectrum (middle, includes mask) and the real and imaginary parts of the time domain (bottom right and left) also displayed.

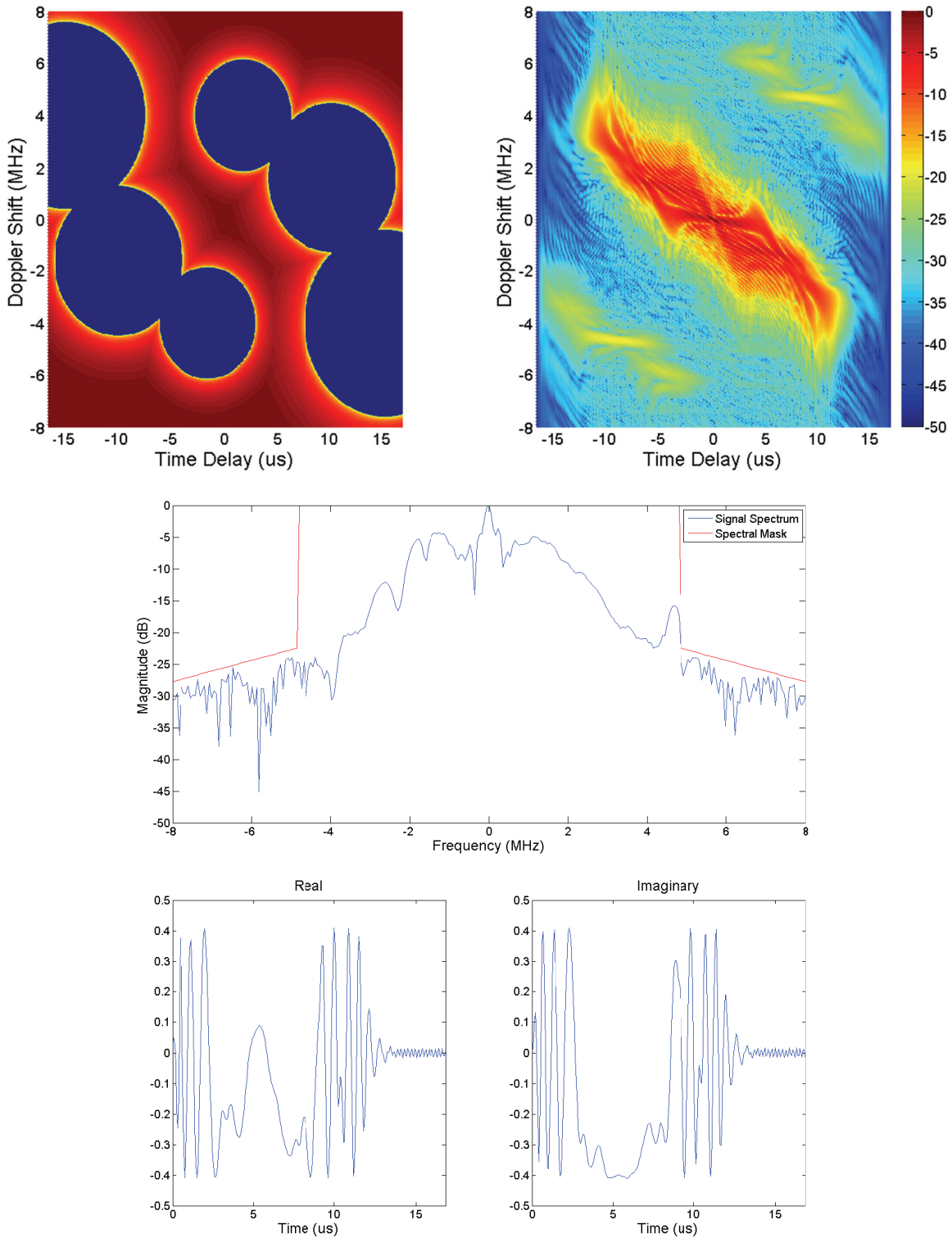


Figure 22: (Measured) Mean-squares optimization result for trial III. The resulting AF magnitude is compared to the minimization function (top), with the spectrum (middle, includes mask) and the real and imaginary parts of the time domain (bottom right and left) also displayed.

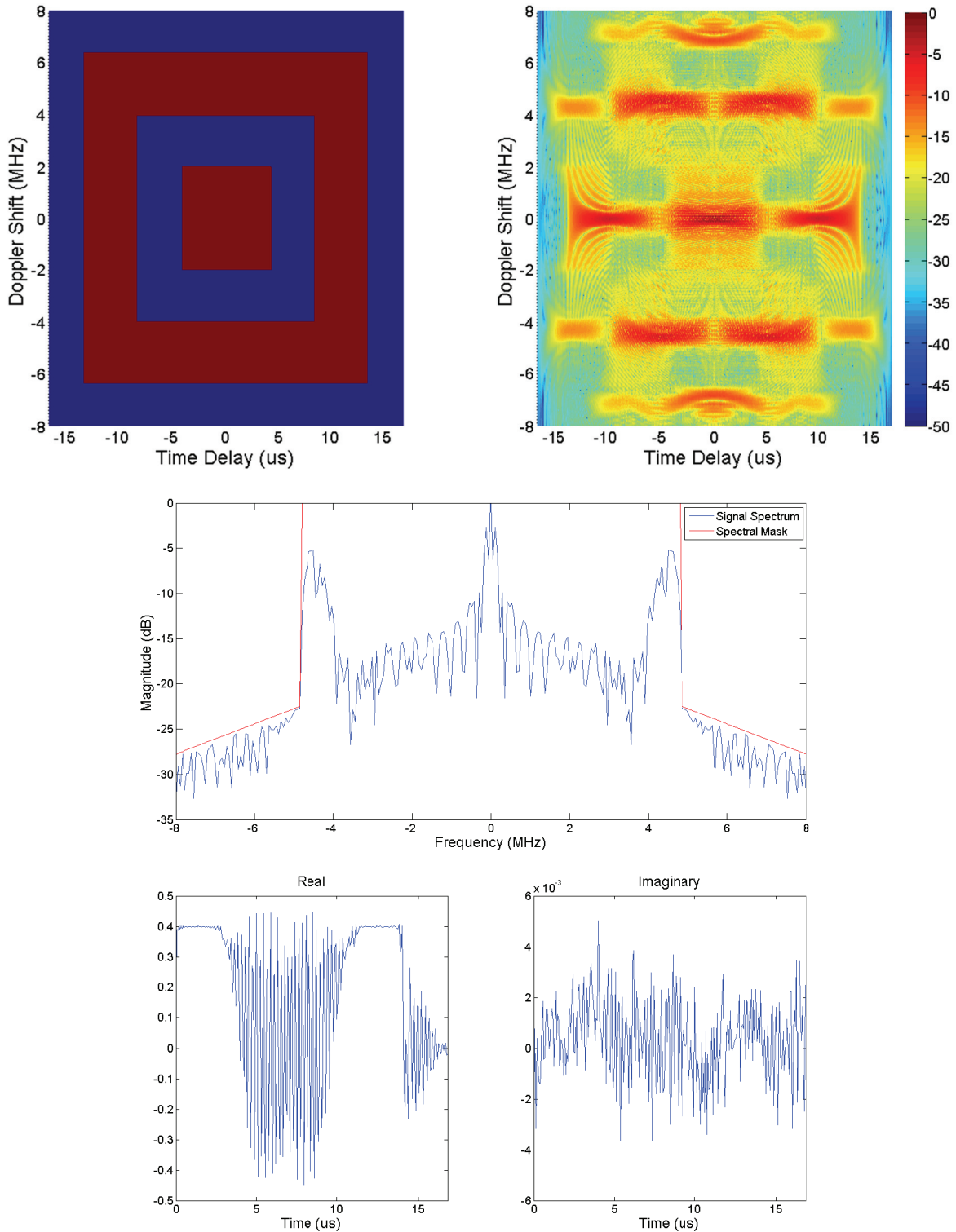


Figure 23: (Measured) Mean-squares optimization result for trial IV. The resulting AF magnitude is compared to the minimization function (top), with the spectrum (middle, includes mask) and the real and imaginary parts of the time domain (bottom right and left) also displayed.

### 4.3.2 Conclusions

As seen in the above results, the projections algorithm does a good job of producing waveforms whose AF volume is constrained to regions specified by a chosen minimization function  $M$ , while also ensuring that the spectrum of the waveform produced conforms to the user-specified spectral mask and the PAPR of the waveform is below a required user-defined value. The results shown are expected; the lower magnitude regions of the synthesized AF correspond well with the lower magnitude regions in the minimization function. Additionally, we see the expected implication of minimizing in certain regions: the higher magnitude regions of the synthesized AF correspond with the higher magnitude regions in the minimization function.

Note that the waveforms produced in these results have higher distance function values than those shown in the previous chapter, when PAPR and spectrum were unconstrained. This result is also expected, because imposing both of these requirements on the synthesized waveform greatly constrains the size of the set of waveforms we can choose from. In the previous chapter, the set of waveforms was mostly unconstrained: any waveform with a normalized energy and of a certain temporal length and bandwidth which was in the support of the AF was acceptable. Constraining the set of waveforms in both the potential amplitude space and the potential frequency space will reduce the size of the set of acceptable waveforms, thus making it more likely for convergence to occur at a greater distance from the set of minimization functions.

Building off of the algorithm outlined in Chapter 3, techniques were examined which guarantee that the synthesized waveform meets user-specified spectral and PAPR constraints. The algorithm is outlined below.

- 
1. Algorithm 2 Waveform synthesis via alternating projections for AF optimization with constraints on PAPR and spectrum
- 
2. **Input:** Minimization function  $M(\tau, u)$ , initial AF  $\chi_{x_0}(\tau, u)$ , # iterations, optimization type,  $T, B$ , desired energy  $E$ , desired PAPR  $\Gamma$ , and spectral mask  $S_m$
  3. **Output:** Optimum waveform  $x_{opt}(t)$
  4. **for**  $n = 0 : \# \text{ iterations}$
  5.     **if**  $D(\chi_{x_n}, P_{\mathcal{M}}(\chi_{x_n})) < D_{opt}$
  6.          $D_{opt} = D(\chi_{x_n}, P_{\mathcal{M}}(\chi_{x_n}))$
  7.          $x_{opt}(t) = x_n(t)$
  8.     **end if**
  9.      $x_{n+1}(t) = P_{\mathcal{E}}(P_{\mathcal{S}}(P_{\mathcal{M}}(\chi_{x_n}), \chi_{x_n}))$
  10.    **while**  $x_{n+1}^{\text{PAPR}} > \Gamma$  **or**  $|X_{n+1}(f)| > S_m(f)$  **or**  $x_{n+1}^E < E$
  11.        $x_{n+1}(t) = P_{\mathcal{C}}(P_{\mathcal{E}}(P_{\mathcal{Z}}(x_{n+1}(t))))$
  12.    **end while**
  13. **end for**
  14. Return  $x_{opt}(t)$
-

## CHAPTER FIVE

### Conclusions

An algorithm has been presented which uses projections to synthesize radar waveforms which have desired range-Doppler resolution properties under user-defined PAPR and spectral constraints. This algorithm will allow for real-time radar waveform synthesis which can respond to changes in the targets' locations and adaptively prioritize the importance of the waveform's accuracy, power amplifier efficiency, and bandwidth. Based on results from the unconstrained optimization in Chapter Three and the constrained optimization in Chapter Four, a tradeoff between the quality of the synthesized waveform's AF and the degree to which PAPR and spectrum is constrained is apparent. This tradeoff can also be theoretically understood by realizing that constraining the set of waveforms to those with acceptable PAPR and bandwidth will reduce the size of the set, which likely further separates the set of minimized functions to the set of associated AFs. In addition to PAPR and bandwidth requirements, the algorithm can easily synthesize waveforms with notched spectrums or non-uniform frequency magnitude in its band based on the spectral mask given as an input.

This work is novel in several ways, most notably in the approaches which allow it to be very robust. Unlike previous works [41] [26] [27] [34] [40] [23] [24] [25] which often use a library of basis functions or pulses to construct waveforms, no prior domain knowledge is required for the algorithm to converge to a useful solution. Additionally, the minimization function on which the algorithm optimizes is very general, in that it does not necessarily need to conform to typical AF properties for convergence as is

required in some other works [23] [24]. Additionally, while some works focus on the autocorrelation properties in either range or Doppler [34] [58], the entirety of the support on the range-Doppler plane for a waveform is considered. Some works also focus on providing a more general AF [41] [27] whose shape resembles that of a thumbtack, while this work allows for adaptive design based on the target environment. These two approaches may be well-suited for combination in a practical radar system, with waveforms having the more general AF shape used to come up with an initial target location map which can be used to construct a minimization function which will be used to construct a more custom waveform using this approach.

One potential issue with this approach is that the nonlinearities of the high power amplifier are not taken into account when synthesizing the waveform. Not considering the effects of the amplifier has several consequences. Firstly, the amplifier non-linearities may cause intermodulation distortion which can result in spectral spreading, creating potential to interfere with adjacent bands. Secondly, our previous work [59] has shown that these non-linearities will have a subsequent impact on the output waveform's AF, which will likely have a negative effect on the quality of the synthesized AF's adherence to the desired minimization function. This is an issue that should be taken into consideration in the continuing progression of this work.

The spectral consequences discussed above may be remedied by applying load-pull based circuit optimization techniques which have been developed concurrently with this research in Baylor's Wireless and Microwave Circuits and Systems lab [60] [61] [62] [63] [64] [51]. These techniques alter circuit parameters to optimize the power added efficiency and adjacent channel power ratio of the system. While preventing spectral

spreading in the waveform optimization process would be ideal, cascading the waveform synthesis algorithm with the load-pull optimization should minimize the effect of spectral spreading by finding a circuit configuration with a spectrally compliant output. This leads us to the overall goal of this work: providing a joint waveform and circuit optimization. A joint optimization would be able to simultaneously adjust the waveform and circuit parameters in response to changes in the operating environment and would be a fantastic contribution towards a cognitive radar system.

## BIBLIOGRAPHY

- [1] P. M. Woodward, *Probability, Information Theory and Radar*, Pergamon, 1953.
- [2] T. Tsao, M. Slamani, P. Varshney, D. Weiner, H. Schwarzlander, "Ambiguity function for a bistatic radar," *IEEE Transactions on Aerospace and Electronic Systems*, vol. 33, no. 3, pp. 1041-1051, 1997.
- [3] D. A. Swick, "A review of wideband ambiguity functions," Naval Research Lab, Washington DC, 1969.
- [4] David C. Lush and Dean Hudson, "Ambiguity function analysis of wideband radars," in *Proceedings of the 1991 IEEE National Radar Conference*, 1991.
- [5] Muhammad Dawood and Ram M. Narayanan, "Ambiguity function of an ultrawideband random noise radar," *Antennas and Propagation Society International Symposium*, vol. 4, pp. 2142-2145, 2000.
- [6] M. I. Skolnik, *Introduction to Radar Systems*, 2nd ed., New York: McGraw-Hill, 1980.
- [7] Eustice, Dylan; Baylis, Charles; Marks II, Robert, "Woodward's Ambiguity Function: From Foundations to Applications," in *Texas Symposium*, Waco, 2015.
- [8] M. Cheney, "A mathematical tutorial on synthetic aperture radar," *SIAM review*, vol. 43, no. 2, pp. 301-312, 2001.
- [9] Harold Szu, J. A. Blodgett, "Wigner distribution and ambiguity function," *Optics in Four Dimensions*, vol. 65, no. 1, pp. 355-381, 1980.
- [10] W. Mecklenbrauker, "A tutorial on non-parametric bilinear time-frequency signal representations," in *Time and frequency representation of signals and systems*, Vienna, Springer, 1989, pp. 11-68.
- [11] K. D. e. a. Merkel, "Multi-Gigahertz radar range processing of baseband and RF carrier modulated signals in Tm: YAG," *Journal of luminescence*, vol. 107, no. 1, pp. 62-74, 2004.
- [12] Yang, Yang, and Rick S. Blum, "MIMO radar waveform design based on mutual information and minimum mean-square error estimation," *Aerospace and Electronic Systems, IEEE Transactions*, vol. 43, no. 1, pp. 330-343, 2007.

- [13] B. Friedlander, "Waveform design for MIMO radars," *Aerospace and Electronic Systems, IEEE Transactions*, vol. 43, no. 3, pp. 1227-1238, 2007.
- [14] Censor, Ron Aharoni and Yair, "Block-Iterative Projection Methods for Parallel Computation of Solutions to Convex Feasibility Problems," *Linear Algebra and Its Applications*, vol. 120, pp. 165-175, 1989.
- [15] Bauschke, Heinz H., and Jonathan M. Borwein, "On projection algorithms for solving convex feasibility problems," *SIAM review*, vol. 38, no. 3, pp. 367-426, 1996.
- [16] Combettes, P. L., "Hilbertian convex feasibility problem: Convergence of projection methods," *Applied Mathematics and Optimization*, vol. 35, no. 3, pp. 311-330, 1997.
- [17] Birgin, Ernesto G., José Mario Martínez, and Marcos Raydan, "Nonmonotone spectral projected gradient methods on convex sets," *SIAM Journal on Optimization*, vol. 10, no. 4, pp. 1196-1211, 2000.
- [18] Hero III, Alfred O., and Doron Blatt, "Sensor network source localization via projection onto convex sets (POCS)," in *IEEE International Conference on Acoustics, Speech, and Signal Processing*, 2005.
- [19] Stark, Henry, and Peyma Oskoui, "High-resolution image recovery from image-plane arrays, using convex projections," *JOSA A*, vol. 6, no. 11, pp. 1715-1726, 1989.
- [20] Park, J., Park, D. C., Marks, R. J., & El-Sharkawi, M., "Recovery of image blocks using the method of alternating projections," *IEEE Transactions on Image Processing*, vol. 14, no. 4, pp. 461-474, 2005.
- [21] Cho, S., Lee, S., Marks II, R. J., Oh, S., Sutlief, S. G., & Phillips, M. H., "Optimization of intensity modulated beams with volume constraints using two methods: Cost function minimization and projections onto convex sets," *Medical Physics*, vol. 25, no. 4, pp. 435-443, 1998.
- [22] R. J. Marks, *Handbook of Fourier analysis and its applications*, London: Oxford University Press, 2009.
- [23] Devlin, Keith, *The joy of sets: fundamentals of contemporary set theory*, Springer Science & Business Media, 2012.
- [24] Ferreirós, José, *Labyrinth of thought: a history of set theory and its role in modern mathematics*, Springer Science and Business Media, 2008.

- [25] Wolf, John D.; Lee, Gary M.; Suyo, Charles E., "Radar Waveform Synthesis by Mean-Square Optimization Techniques," *IEEE Transactions on Aerospace and Electronic Systems*, Vols. AES-5, No. 4, pp. 611-619, 1968.
- [26] C. H. Wilcox, "The Synthesis Problem for Radar Ambiguity Functions," Tech. Summary Report No. 157, Mathematics Research Center, University of Wisconsin, Madison, Wisconsin, 1960.
- [27] S. M. Sussman, "Least-square synthesis of radar ambiguity functions," *Information Theory, IRE Transactions*, vol. 8, pp. 246-254, 1962.
- [28] Nehorai, Satyabrata Sen and Arye, "Adaptive Design of ODFM Radar Signal With Improved Wideband Ambiguity Function," *IEEE Transactions on Signal Processing*, vol. 58, no. 2, pp. 928-933, 2010.
- [29] I. Gladkova, D. Chebanov, "On a New Extension of Wilcox's Method," *WSEAS Transactions on Mathematics*, vol. 3, no. 1, 2004.
- [30] I. Gladkova, D. Chebanov, "On the Synthesis Problem for a Waveform Having a Nearly Ideal Ambiguity Surface," in *RADAR 2004 - International Conference on Radar Systems*, Philadelphia, 2004.
- [31] Costas, John P., "A study of a class of detection waveforms having nearly ideal range—doppler ambiguity properties," *Proceedings of the IEEE*, vol. 72, no. 8, pp. 996-1009, 1984.
- [32] Levanon, Nadav, and Eli Mozeson, *Radar signals*, John Wiley and Sons, 2004.
- [33] N. Levanon, *Radar Principles*, New York: Wiley-Interscience, 1988.
- [34] Lacomme, Philippe, *et al.*, *Air and spaceborne radar systems: An introduction*, William Andrew, 2001.
- [35] Levanon, N., *Radar Principles*, New York: Wiley-Interscience, 1988.
- [36] M. Albulet, *RF Power Amplifiers*, SciTech Publishing, 2001.
- [37] K. K. Clark and D. T. Hess, *Communication Circuits: Analysis and Design*, Boston: Addison-Wesley, 1971.
- [38] N. O. Sokal, I. Novak, J. Donohue, "Classes of RF Power Amplifiers A Through S, How They Operate, and When to Use Them," in *RF Expo West*, San Diego, CA, 1995.
- [39] F. E. Terman, *Radio Engineering*, New York: McGraw-Hill, 1947.

- [40] Sebt, M. A.; Sheikhi, A.; Nayebi, M. M., "Orthogonal Frequency-Division Multiplexing Radar Signal Design with Optimised Ambiguity Function and Low Peak-to-Average Power Ratio," *IET Radar, Sonar, and Navigation*, vol. 3, no. 2, pp. 122-132, 2008.
- [41] Robert L. Boylestad, Louis Nashelsky, *Electronic Devices and Circuit Theory*, Prentice Hall, 1999.
- [42] Matthew Fellows, Charles Baylis, Lawrence Cohen, and Robert J. Marks II, "Radar Waveform Optimization to Minimize Spectral Spreading and Achieve Target Detection," in *Texas Symposium on Wireless and Microwave Circuits and Systems*, Waco, TX, 2013.
- [43] Joseph Mitola III, Gerald Q. Maguire Jr, "Cognitive radio: making software radios more personal," *Personal Communications, IEEE*, vol. 6, no. 4, pp. 13-18, 1999.
- [44] S. Haykin, "Cognitive radar: a way of the future," *Signal Processing Magazine, IEEE*, vol. 23, no. 1, pp. 30-40, 2006.
- [45] J. R. Guerci, *Cognitive Radar: The Knowledge-aided Fully Adaptive Approach*, London: Artech House, 2010.
- [46] Zhou, Liu-Lei, Hong-Bo Zhu, and Nai-Tong Zhang, "Iterative solution to the notched waveform design in cognitive ultra-wideband radio system," *Progress In Electromagnetics Research*, vol. 75, pp. 271-284, 2007.
- [47] Chakravarthy, Vasu D., *et al.*, "Cognitive radio-an adaptive waveform with spectral sharing capability," *Wireless Communications and Networking Conference, IEEE*, vol. 2, pp. 724-729, 2005.
- [48] Sheng, Hongsan, Philip Orlik, Alexander M. Haimovich, Leonard J. Cimini Jr, and Jinyun Zhang, "On the spectral and power requirements for ultra-wideband transmission," *IEEE International Conference on Communications*, vol. 1, pp. 738-742, 2003.
- [49] Parr, Brent, ByungLok Cho, Kenneth Wallace, and Zhi Ding, "A novel ultra-wideband pulse design algorithm," *IEEE Communications Letters*, vol. 7, no. 5, pp. 219-221, 2003.
- [50] Wang, Xianbin, Tjeng Thiang Tjhung, and C. S. Ng, "Reduction of peak-to-average power ratio of OFDM system using a companding technique," *IEEE Transactions on Broadcasting*, vol. 45, no. 3, pp. 303-307, 1999.
- [51] Biggs, Shannon D. Blunt and Casey R., "Practical Considerations for Intra-Pulse Radar-Embedded Communications," in *International Waveform Diversity and Design*, Kissimmee, FL, 2009.

- [52] Yantham, Shannon D. Blunt and Padmaja, "Waveform Design for Radar-Embedded Communications," in *Waveform Diversity and Design*, Pisa, Italy, 2007.
- [53] Selesnick, I. W.; Pillai, S. U., "An Iterative Algorithm for the Construction of Notched Chirp Signals," in *IEEE Radar Conference*, Washington DC, 2010.
- [54] Selesnick, I. W.; Pillai, S. U., "Chirp-Line Transmit Waveforms with Multiple Frequency-Notches," in *IEEE Radar Conference*, Kansas City, MO, 2011.
- [55] Rowe, Wayne, Petre Stoica, and Jian Li, "Spectrally Constrained Waveform Design [sp Tips&Tricks]," *IEEE Signal Processing Magazine*, vol. 31, no. 3, pp. 157-162, 2014.
- [56] Charles Baylis, Matthew Fellows, Lawrence Cohen, Robert Marks, "Solving the Spectrum Crisis," *IEEE Microwave Magazine*, pp. 94-107, 2014.
- [57] Charles Baylis, Matthew Fellows, Matthew Flachsbart, Jennifer Barlow, Joseph Barkate, and Robert J. Marks II, "Enabling the Internet of Things: Reconfigurable power amplifier techniques using intelligent algorithms and the Smith tube," in *Circuits and Systems Conference*, Dallas, 2014.
- [58] Joseph Barkate, Matthew Fellows, Jennifer Barlow, Charles Baylis, and Robert J. Marks, "The Power Smith Tube: Joint optimization of power amplifier input power and load impedance for power-added efficiency and adjacent-channel power ratio," in *IEEE 16th Annual Wireless and Microwave Technology Conference*, 2015.
- [59] Josh Martin, Matthew Moldovan, Charles Baylis, Robert Marks, Lawrence Cohen, Jean de Graaf, "Radar Chirp Waveform Selection and Circuit Optimization Using ACPR Load-Pull Measurements," in *IEEE 13th Annual Wireless and Microwave Technology Conference*, 2012.
- [60] Matthew Fellows, Charles Baylis, Lawrence Cohen, Robert Marks II, "Real-Time Load Impedance Optimization for Radar Spectral Mask Compliance and Power Efficiency," *IEEE Transactions on Aerospace and Electronic Systems*, vol. 51, no. 1, pp. 591-600, 2015.
- [61] M. Fellows, *Waveform and Circuit Optimizations to Provide Spectral Compliance for Cognitive Radar*, Waco, TX: Baylor University, 2013.
- [62] Kyoungsoon Yang, George Haddad, Jack East, "High-Efficiency Class-A Power Amplifiers with a Dual-Bias-Control Scheme," *IEEE Transactions on Microwave Theory and Techniques*, vol. 47, no. 8, 1999.

[63] Zimek, A.; Schubert, E.; Kriegel, HP, "A survey on unsupervised outlier detection in high-dimensional numerical data," *Statistical Analysis and Data Mining*, vol. 5, no. 5, p. 363–387, 2012.

[64] R. E. Bellman, *Dynamic programming*, Princeton University Press, 1957.